

1 **Potent neutralization of SARS-CoV-2 variants of concern by an antibody with a unique**
2 **genetic signature and structural mode of spike recognition**

3

4 Kevin J. Kramer^{1,2,*}, Nicole V. Johnson^{3,*}, Andrea R. Shiakolas^{1,2}, Naveenchandra
5 Suryadevara¹, Sivakumar Periasamy^{4,5}, Nagarajan Raju¹, Jazmean K. Williams⁶, Daniel Wrapp³,
6 Seth J. Zost¹, Clinton M. Holt^{1,7}, Ching-Lin Hsieh³, Rachel E. Sutton¹, Ariana Paulo¹, Edgar
7 Davidson⁶, Benjamin J. Doranz⁶, James E. Crowe Jr^{1,8}, Alexander Bukreyev^{4,5}, Robert H.
8 Carnahan^{1,8}, Jason S. McLellan^{3,#}, Ivelin S. Georgiev^{1,2,9,10,11,12,13,#}

9

10 ¹Vanderbilt Vaccine Center, Vanderbilt University Medical Center, Nashville, TN, 37232, USA

11 ²Department of Pathology, Microbiology, and Immunology, Vanderbilt University Medical Center,
12 Nashville, TN, 37232, USA

13 ³Department of Molecular Biosciences, The University of Texas at Austin, Austin, TX, 78712,
14 USA

15 ⁴Department of Pathology, University of Texas Medical Branch at Galveston, Galveston, TX
16 77555, USA

17 ⁵Galveston National Laboratory, University of Texas Medical Branch at Galveston, Galveston,
18 TX 77555, USA

19 ⁶Integral Molecular, Philadelphia, PA 19104, USA

20 ⁷Program in Chemical and Physical Biology, Vanderbilt University Medical Center, Nashville,
21 TN, 37232, USA

22 ⁸Department of Pediatrics, Vanderbilt University Medical Center, Nashville, TN, 37232, USA

23 ⁹Vanderbilt Institute for Infection, Immunology, and Inflammation, Vanderbilt University Medical
24 Center, Nashville, TN, 37232, USA

25 ¹⁰Department of Electrical Engineering and Computer Science, Vanderbilt University Medical
26 Center, Nashville, TN, 37232, USA

27 ¹¹Center for Structural Biology, Vanderbilt University, Nashville, TN, 37232, USA

28 ¹²Program in Computational Microbiology and Immunology, Vanderbilt University Medical
29 Center, Nashville, TN, 37232, USA

30 ¹³Lead Contact

31 *These authors contributed equally

32 #Address correspondence to: ivelin.georgiev@vanderbilt.edu and jmclellan@austin.utexas.edu

33 **Abstract**

34 The emergence of novel SARS-CoV-2 lineages that are more transmissible and
35 resistant to currently approved antibody therapies poses a considerable challenge to the clinical
36 treatment of COVID-19. Therefore, the need for ongoing discovery efforts to identify broadly
37 reactive monoclonal antibodies to SARS-CoV-2 is of utmost importance. Here, we report a
38 panel of SARS-CoV-2 antibodies isolated using the LIBRA-seq technology from an individual
39 who recovered from COVID-19. Of these antibodies, 54042-4 showed potent neutralization
40 against authentic SARS-CoV-2 viruses, including variants of concern (VOCs). A cryo-EM
41 structure of 54042-4 in complex with the SARS-CoV-2 spike revealed an epitope composed of
42 residues that are highly conserved in currently circulating SARS-CoV-2 lineages. Further,
43 54042-4 possesses unique genetic and structural characteristics that distinguish it from other
44 potentially neutralizing SARS-CoV-2 antibodies. Together, these findings motivate 54042-4 as a
45 lead candidate for clinical development to counteract current and future SARS-CoV-2 VOCs.

46 **Introduction**

47 The COVID-19 pandemic caused by a novel coronavirus from the *Sarbecovirus* genus,
48 SARS-CoV-2, spawned an unprecedented global research effort dedicated to therapeutic
49 countermeasure development resulting in rapid US FDA Emergency Use Authorization (EUA)
50 for vaccines and monoclonal antibodies (Jones et al., 2021; Weinreich et al., 2021). The primary
51 target for vaccine and antibody therapeutic development is the SARS-CoV-2 spike (S) protein,
52 which facilitates host-cell attachment and entry (Wrapp et al., 2020). The emergence of distinct
53 viral lineages that accumulate substitutions in the S protein pose a significant threat to the
54 countermeasures currently approved for clinical use (Chen et al., 2021; Wang et al., 2021).
55 Continued genomic surveillance and persistent efforts to identify novel antibodies with distinct
56 binding modes and mechanisms of action are crucial to maintain availability of therapeutics in
57 the event of further neutralization-escape by SARS-CoV-2 variants of concerns (VOCs).

58 SARS-CoV-2 spike is a class I viral fusion protein that is a trimer of heterodimers
59 composed of S1 and S2 subunits (Wrapp et al., 2020). S1 initiates attachment to the receptor
60 angiotensin-converting enzyme 2 (ACE2), whereas S2 drives membrane fusion by refolding
61 from a prefusion to postfusion conformation (Li, 2016; Tortorici and Veesler, 2019). The primary
62 contact of ACE2 and spike is in the receptor-binding domain (RBD) of the S1 subunit, which is
63 composed of a receptor binding motif (RBM) and RBD core. The three RBDs within each spike
64 can adopt an ACE2-accessible “up” conformation and an ACE2-inaccessible “down”
65 conformation via a hinge-like motion (Shang et al., 2020). As a result, although multiple
66 neutralizing epitopes on spike have been identified (Brouwer et al., 2020; Chi et al., 2020;
67 Suryadevara et al., 2021; Zost et al., 2020), the RBD serves as the dominant target of
68 neutralizing antibodies via antagonism of ACE2 binding (Piccoli et al., 2020).

69 Neutralizing antibodies targeting the RBD have been characterized extensively and
70 partition into different classes based on binding mode, ACE2 interface overlap, and cross-

71 reactivity with other *Sarbecoviruses*. For example, neutralizing antibodies predominantly
72 encoded by IGHV3-53 and IGHV3-66 have epitopes directly covering the ACE2 interaction
73 footprint in the RBM (Yuan et al., 2020a). Examples of this class of antibodies are clinical EUA
74 candidates REGN10933 and COV2-2196 (Hansen et al., 2020; Zost et al., 2020). Antibodies
75 that bind the RBM but are more distal to the ACE2 interface form another distinct class that
76 includes REGN10987 and COV2-2130 (Dong et al., 2021; Hansen et al., 2020). Additionally,
77 antibodies such as CR3022 and ADG-2 that cross-react with other coronaviruses comprise a
78 more diverse group that target conserved residues in the RBD-core (Pinto et al., 2020; Wec et
79 al., 2020; Yuan et al., 2020b).

80 The continued transmission of SARS-CoV-2 in the human population has led to the
81 evolution of VOCs with increased transmissibility and resistance to available medical
82 countermeasures (Alpert et al., 2021; Kuzmina et al., 2021). Some of the most consequential
83 amino acid substitutions observed so far have occurred in the RBD, particularly N501Y in the
84 B.1.1.7, B.1.351, and P.1 lineages, and the additional combination of K417N/T and E484K in
85 the P.1 and B.1.351 lineages. In particular, N501Y is thought to increase affinity for ACE2 (Starr
86 et al., 2020) potentially resulting in increased infectivity, whereas E484K disrupts the antigenic
87 landscape of the RBD that can lead to substantial decreases in neutralization titers (Hoffmann
88 et al., 2021; Wang et al., 2021). In some cases, SARS-CoV-2 VOCs also escape neutralization
89 by polyclonal antibodies in the serum from vaccine recipients and individuals previously infected
90 with SARS-CoV-2 (Chen et al., 2021; Wang et al., 2021). These observations highlight the
91 critical need for a wide range of potentially neutralizing antibodies insensitive to substitutions
92 arising in VOCs.

93 To address this challenge, we applied LIBRA-seq, a recently developed antibody-
94 discovery technology (Setliff et al., 2019; Shiakolas et al., 2020), to interrogate the B cell
95 repertoire of an individual who had recovered from COVID-19. Our efforts led to the discovery of

96 a potentially neutralizing antibody, designated 54042-4, which uses a unique genetic signature
97 and structural mode of SARS-CoV-2 RBD recognition to maintain neutralization potency to
98 known VOCs. Antibody 54042-4 therefore may serve as a viable candidate for further
99 prophylactic or therapeutic development for protection against a broad range of SARS-CoV-2
100 variants.

101

102 **RESULTS**

103 **Identification of SARS-CoV-2-neutralizing antibodies by LIBRA-seq**

104 To identify SARS-CoV-2 S-directed antibodies, we utilized LIBRA-seq (Linking B Cell
105 receptor to antigen specificity through sequencing), a technology that enables high-throughput
106 simultaneous determination of B cell receptor sequence and antigen reactivity at the single-cell
107 level, expediting the process of lead candidate selection and characterization (Setliff et al.,
108 2019). The LIBRA-seq antigen-screening library included SARS-CoV-2 spike stabilized in a
109 prefusion conformation (Hsieh et al., 2020), along with antigens from other coronaviruses and
110 negative-control antigens. Antigen-specific B cells were isolated from a donor with potentially
111 neutralizing antibodies in serum (1:258 NT₅₀) three months after infection confirmed by nasal
112 swab RT-PCR testing for SARS-CoV-2 (**Supplemental Figure 1A**). Of the 73 IgG⁺ B cells with
113 high LIBRA-seq scores (≥ 1) for SARS-CoV-2 S (**Figure 1A, Supplemental Figure 1B**), we
114 chose nine lead candidates with diverse sequence characteristics, CDRH3 length, and germline
115 V gene usage for characterization as recombinant monoclonal antibodies (**Figure 1B**). Binding
116 to SARS-CoV-2 S by ELISA was confirmed for eight of these antibodies, with the only exception
117 being antibody 54042-2, in agreement with its lower LIBRA-seq score (**Figure 1B,**
118 **Supplemental Figure 1C**). Five of these antibodies showed SARS-CoV-2 neutralization activity
119 in a high-throughput neutralization screen using a live chimeric VSV displaying SARS-CoV-2

120 spike protein (Case et al., 2020) (**Figure 1B**). Full dose-response neutralization curves in the
121 chimeric VSV assay were obtained for four of these five antibodies, with antibody 54042-4
122 showing the best potency, at a half-maximal inhibitory concentration (IC_{50}) of 9 ng/mL (**Figure**
123 **1C**).

124

125 **Antibody 54042-4 targets the SARS-CoV-2 receptor-binding domain**

126 Because of the potent (≤ 10 ng/mL) virus neutralization observed for 54042-4, we
127 selected this antibody for further characterization. ELISAs performed with purified RBD, NTD,
128 S1, and S2 proteins revealed 54042-4 IgG bound to the SARS-CoV-2 S1 subunit as well as the
129 RBD (**Figure 2A, Supplemental Figure 2**). To determine the affinity of the antibody-antigen
130 binding interaction, biolayer interferometry experiments were performed by measuring the
131 association and dissociation kinetics of immobilized 54042-4 IgG binding to a soluble protein
132 comprising the RBD and subdomain-1 (SD1) of the SARS-CoV-2 S protein. Curve-fitting
133 resulted in a calculated K_D of 21.8 nM (**Figure 2B**). Given the neutralization potency of 9 ng/mL
134 (60 pM), these data suggest that the IgG avidly binds to the S protein on the surface of the
135 virus. To assess whether 54042-4 neutralizes viral infection by directly competing with ACE2, a
136 receptor-blocking assay was performed by testing the competition of 54042-4 with soluble ACE2
137 for binding to SARS-CoV-2 S. The results demonstrated that 54042-4 inhibits interaction of
138 ACE2 to SARS-CoV-2 S protein, unlike the control antibodies CR3022, an extensively
139 characterized SARS-CoV antibody that binds a cryptic epitope in the RBD (Yuan et al., 2020b),
140 and the influenza hemagglutinin-specific 3602-1707 (Setliff et al., 2019) (**Figure 2C**). Next, we
141 performed competition ELISA to determine if 54042-4 competes for binding with three other
142 RBD-directed antibodies with distinct epitopes. These antibodies included COV2-2196 and
143 COV2-2130, which form the basis of AZD7442, an antibody cocktail currently under
144 investigation in clinical trials for COVID-19 treatment and prevention (ClinicalTrials.gov

145 Identifiers: NCT04625725, NCT04723394, NCT04518410, and NCT04501978) and CR3022.
146 The competition experiment showed that 54042-4 competed for binding to SARS-CoV-2 S
147 protein with COV2-2130, but not COV2-2196 or CR3022 (**Figure 2D**). Together, these results
148 suggest that 54042-4 targets an epitope on SARS-CoV-2 RBD that at least partially overlaps
149 with the binding sites for both ACE2 and other potentially neutralizing RBD antibodies.

150

151 **54042-4 binds the apex of the SARS-CoV-2 RBD in the down conformation**

152 To gain a better understanding of the recognition of SARS-CoV-2 S by antibody 54042-
153 4, we determined a 2.7 Å resolution cryo-EM structure of the 54042-4 antigen-binding fragments
154 (Fabs) bound to the SARS-CoV-2 S extracellular domain (ECD) modified so that all three RBDs
155 were disulfide-locked in the down conformation (Henderson et al., 2020) (**Figure 3A**). Local
156 refinement of one RBD bound to a 54042-4 Fab was performed to improve the interpretability of
157 the map at the binding interface, resulting in a local 3D reconstruction with a resolution of 2.8 Å
158 (**Figure 3B**). The structure revealed that 54042-4 forms an extensive interface with the RBD,
159 making contacts through the CDRL1, CDRL3, and all three CDRs of the heavy chain, to form a
160 clamp around the apex of the RBM saddle (**Figure 3C,D, Supplemental Figure 3**). The primary
161 interactions involve RBD residues 439–450, with a network of hydrogen bonds between the
162 54042-4 heavy chain and RBD residues 443–447 (**Figure 3C**). From CDRH3, Ser99 forms a
163 hydrogen bond with RBD residue Ser443, and a hydrogen bond is formed between the
164 mainchain atoms of Phe97 and Val445. From CDRH2, Asp56 forms a hydrogen bond and salt
165 bridge with Lys444, whereas Arg58 forms hydrogen bonds with mainchain atoms from Gly446
166 and Gly447. The CDRH1 contributes a lone residue, Ile32, to the binding interface, forming
167 minor contacts near Leu441. The 54042-4 light chain surrounds the opposite side of this RBD
168 region, mediating interactions primarily through hydrophobic contacts formed by CDRL1 and
169 CDRL3 near RBD residue Val445 (**Figure 3D**). Additional light chain contacts are made with

170 residues 498–500 of the RBD, including a hydrogen bond between His92 of CDRL3 and
171 Thr500, and hydrophobic interactions involving CDRL1 Phe30 and Tyr32. Notably, the complex
172 structure indicated that a number of spike substitutions associated with current VOCs are
173 unlikely to affect recognition by antibody 54042-4. For example, RBD residue Asn501 (present
174 as Tyr501 in several VOCs, including B.1.1.7, B.1.351, and P.1) lies just outside of the 54042-4
175 epitope, whereas the C α atoms of Glu484 (present as Lys484 or Gln484 in, e.g., B.1.351, P.1,
176 and B.1.617) and Leu452 (present as Arg452 in B.1.427) are approximately 18 and 14 Å away
177 from the C α atoms of the nearest 54042-4 residue, respectively (**Figure 3B**).

178

179 **Antibody 54042-4 has a unique genetic signature and structural mode of RBD recognition**

180 Public clonotype sequence signatures (those shared by multiple individuals recovered
181 from COVID-19 infection) have been identified for potently neutralizing SARS-CoV-2 antibodies,
182 including antibodies currently in clinical trials or approved for emergency use (Nielsen et al.,
183 2020; Yuan et al., 2020a). To investigate whether antibody sequences that are closely related to
184 54042-4 can be identified among known SARS-CoV-2 antibodies, we searched the CoV-AbDab
185 database that contains paired heavy-light chain sequences of coronavirus antibodies (Raybould
186 et al., 2021). Notably, antibodies with high sequence identity to the 54042-4 CDRH3 and
187 CDRL3 were not identified, whether or not the search was restricted to the *IGHV2-5* heavy
188 chain and *IGKV1-39* light chain genes utilized by 54042-4 (**Figure 4A**).

189 Next, we compared the 54042-4 epitope to the epitopes of other known SARS-CoV-2
190 antibodies by computing pairwise correlations between the antibody-antigen buried surface
191 areas for 54042-4 against a set of available SARS-CoV-2 antibody-antigen structures. The
192 results revealed significant positive correlations with only four other antibodies:
193 REGN10987(Hansen et al., 2020), 2-7 (Liu et al., 2020), C119 (Barnes et al., 2020), and

194 COVOX-75 (Dejnirattisai et al., 2021) (**Figure 4B**). However, of these four antibodies, COVOX-
195 75 has been reported as not a potent neutralizer (Dejnirattisai et al., 2021). C119 makes
196 substantial contact with residues Asn501 and Glu484, indicating potential susceptibility of this
197 antibody to substitutions at those positions that are currently associated with relatively high
198 substitution rates (**Figure 4C**) and are present in several circulating SARS-CoV-2 VOCs (Alpert
199 et al., 2021; Tegally et al., 2021). Further, both C119 and COVOX-75 have substantial buried
200 surface area interactions with a number of additional residues compared to those in the epitope
201 of 54042-4 (**Figure 4C**), suggesting that these two antibodies would be susceptible to a greater
202 number of potential spike substitutions than 54042-4.

203 We also observed that while the epitopes of antibodies 2-7 and REGN10987 correlate
204 well with that of 54042-4, these antibodies have distinct angles of antigen approach (**Figure**
205 **4D**). To quantify this observation, we aligned the RBDs from the 2-7 and REGN10987 complex
206 structures with the RBD from the 54042-4 structure. Using the antibody coordinates when the
207 respective RBDs were aligned, we computed the root mean square deviations (RMSD) between
208 the C α atoms in the FWR1-FWR3 regions of the antibody heavy and light chains. This resulted
209 in RMSDs of 16.4 Å and 22 Å between 54042-4 versus 2-7 and REGN10987, respectively,
210 confirming the substantial differences in the structural mode of antigen recognition by 54042-4
211 compared to 2-7 and REGN10987. Further, although 54042-4 and 2-7 both originate from the
212 same *IGHV2-5* germline gene and share analogous RBD contacts in the CDRH2 region, these
213 antibodies exhibit different CDRH1 and CDRH3 interactions (**Figure 4E**) and use a different
214 light chain germline gene (*VK1-39* for 54042-4, and *VL2-14* for 2-7). Notably, both 2-7 and
215 REGN10987 have greater interactions with RBD residues 439–441 compared to 54042-4, with
216 buried surface areas of 172, 127, and 60 Å² for 2-7, REGN10987, and 54042-4, respectively
217 (**Figure 4C**), suggesting 2-7 and REGN10987 may be more prone to viral escape in that region.

218 Indeed, the N439K substitution is present in several independent SARS-CoV-2 lineages and
219 has been found to affect binding and neutralization by REGN10987 (Thomson et al., 2021).

220 Together, these data suggest that antibody 54042-4 utilizes a unique genetic signature
221 and structural mode of antigen recognition that are distinct from other known SARS-CoV-2
222 antibodies.

223

224 **Antibody 54042-4 is not affected by current SARS-CoV-2 VOC substitutions**

225 To identify substitutions capable of disrupting binding to antibody 54042-4, we next
226 performed shotgun alanine-scanning mutagenesis of the SARS-CoV-2 RBD (Davidson, 2014).
227 The only substitutions tested that substantially affected binding in comparison to an RBD
228 antibody control were K444A, V445A, G446A, and P499A (**Figure 5A**), which all fall within the
229 54042-4 epitope (**Figure 3C, D, and Supplemental Figure 3A**). Next, to assess the functional
230 effect of substitutions within the 54042-4 epitope, we tested neutralization against VSV-SARS-
231 CoV-2 chimeras containing substitutions at K444R/T/E/N, G446D, or Q498R. These specific
232 substitutions were chosen based on their generation from neutralization-escape experiments
233 with monotreatment at saturating concentration of antibodies COV2-2130 (shown to compete
234 with 54042-4, **Figure 2D**) and COV2-2499 (a known COV2-2130 competitor) (Greaney et al,
235 2021). These experiments revealed that the chimeric VSVs with substitutions at Lys444, Gly446,
236 and Gln498 were resistant to neutralization by 54042-4 (**Figure 5B**). Together, the alanine-
237 scanning and neutralization-escape experiments indicated that 54042-4 recognition of spike
238 may be sensitive to substitutions at residues K444, V445, G446, Q498, and P499. However,
239 analysis of currently circulating SARS-CoV-2 isolates from the GISAID database as of May 6,
240 2021 (Elbe, 2017) revealed that substitutions at these five residue positions are only present at
241 low levels (**Figure 5C**). Further, virtually all of the 54042-4 epitope residues (**Supplemental**

242 **Figure 3A**) are highly conserved in circulating SARS-CoV-2 lineages (**Figure 5C**). The only
243 exception is residue N439, which has a substitution frequency of 2.1% (**Figure 5C**); however,
244 this residue makes only minimal contacts with antibody 54042-4 (**Supplemental Figure 3A**),
245 suggesting that residue N439 may not be critical for 54042-4 recognition of the SARS-CoV-2
246 spike.

247 To investigate the ability of antibody 54042-4 to recognize current SARS-CoV-2 VOCs,
248 we next performed ELISAs to test binding of 54042-4 to RBD proteins containing substitutions
249 found in one or more VOCs. These substitutions included K417N found in many isolates in the
250 B.1.351 lineage, as well as E484K (B.1.351, P.1), N501Y (B.1.1.7, B.1.351, P.1), as well as
251 N439K found in lineages B.1.141 and B.1.258 (Thomson et al., 2021). Notably, antibody 54042-
252 4 bound to these RBD variants at a similar level compared to the binding to the RBD from the
253 Wuhan-1 isolate (**Figure 5D, Supplemental Figure 4A**). These results are consistent with the
254 structural observations that 54042-4 makes only minimal contacts with residue 439, and that
255 none of the other RBD substitutions were at residues in the 54042-4 epitope (**Supplemental**
256 **Figure 3A**). Binding of antibody 54042-4 also was not affected in the context of S ECD proteins
257 that included deletions and substitutions in the S1 domain of the B.1.351 and B.1.1.7 VOCs
258 (**Figure 5D, Supplemental Figure 4B,C**). Importantly, we also tested the ability of 54042-4 to
259 neutralize authentic SARS-CoV-2 USA-WA1, B.1.1.7, and B.1.351 SARS-CoV-2 variants.
260 Consistent with the ELISA data, 54042-4 neutralized each virus potently with IC₅₀s of 3.2, 7.2,
261 and 13 ng/mL, respectively (**Figure 5E**). Together, these data indicate that 54042-4 can be an
262 effective countermeasure against currently circulating SARS-CoV-2 variants.

263

264 **Discussion**

265 SARS-CoV-2 neutralizing antibody discovery efforts have produced an extensive panel
266 of antibodies that show a wide range of functional effects, yet most antibodies discovered to
267 date cluster into several classes based on RBD-binding orientation, ACE2 antagonism, and
268 cross-reactivity to related SARS-like coronaviruses (Greaney et al, 2021). Here, we report the
269 identification of 54042-4, an antibody that exhibited ultra-potent SARS-CoV-2 neutralization
270 against USA-WA1 as well as the currently circulating VOCs B.1.1.7 and B.1.351. While the
271 epitope of antibody 54042-4 showed partial overlap with that of several other known RBD
272 antibodies, our findings revealed an overall unique mode of SARS-CoV-2 spike recognition,
273 paired with an uncommon genetic signature that distinguishes 54042-4 from other SARS-CoV-2
274 antibodies. Notably, important differences were observed even for the four antibodies with the
275 highest epitope correlations to 54042-4, with all four of these antibodies exhibiting substantially
276 greater contacts with one or more known residues associated with currently circulating VOCs
277 (**Figure 4C**). The discovery of antibody 54042-4 is therefore a unique addition to the limited set
278 of antibodies with a high potential for effectively counteracting current SARS-CoV-2 VOCs.

279 The increased spread of several SARS-CoV-2 VOCs over the past few months has
280 emphasized the need for continued surveillance of vaccine efficacy against the evolving virus
281 targets. The increased transmission rates of the B.1.1.7 lineage are likely a product of enhanced
282 ACE2 affinity for the SARS-CoV-2 RBD (Starr et al., 2020), and not a result of escape from pre-
283 existing antibodies in convalescent or vaccinated individuals (Wang et al., 2021; Xie et al.,
284 2021). Variants that encode the E484K substitution appear to pose a significantly higher risk of
285 neutralization escape in vaccine recipients and individuals who have recovered from COVID-19
286 (Wang et al., 2021). Indeed, the rise of cases associated with the P.1 variant that harbors the
287 E484K substitution (among others) in Manaus, Brazil is on a dangerous trajectory, despite
288 having a 76% population seropositivity rate dating back to March 2020 (Sabino et al., 2021). In
289 the context of vaccination, early vaccine trial data for Novavax against the B.1.351 lineage in

290 South Africa (also encoding the E484K substitution) demonstrated a significant decrease in
291 efficacy (Wadman, 2021). These observations underscore the ongoing need for genomic
292 surveillance to monitor the emergence and spread of new SARS-CoV-2 variants and their
293 effects on population immunity.

294 In addition to vaccines, antibody therapeutics can play an important role for treating
295 SARS-CoV-2 infections. Given the unknown future trajectory of the pandemic and the potential
296 for emergence of VOCs that may escape neutralization by vaccine-elicited immunity, the
297 development of a wide array of candidate antibody therapeutics that are insensitive to
298 substitutions found in major VOCs may prove critical in the fight against COVID-19. However,
299 current VOCs have already shown an ability to escape neutralization by a number of antibodies
300 in clinical development (Chen et al., 2021; Wang et al., 2021). In contrast, our binding,
301 neutralization, and structural data suggest that antibody 54042-4 is capable of avoiding all of the
302 current major substitutions in circulating VOCs. Combined with those observations, the unique
303 features of 54042-4 in comparison to other SARS-CoV-2 antibodies motivate further clinical
304 development of this antibody to complement the existing pool of therapeutic countermeasures.
305 As SARS-CoV-2 virus evolution continues due to various factors, such as a lack of vaccine
306 access and the associated delayed vaccine rollout to underserved parts of the world, new VOCs
307 are likely to keep emerging, with the potential to decrease or even abrogate protection induced
308 by current vaccines. Antibody therapeutic development, especially focusing on broad protection
309 against diverse SARS-CoV-2 variants, is therefore of continued significance.

310 **METHODS**

311 **Donor Information**

312 The donor had previous laboratory-confirmed COVID-19, 3 months prior to blood collection. The
313 studies were reviewed and approved by the Institutional Review Board of Vanderbilt University
314 Medical Center. The sample was obtained after written informed consent was obtained.

315

316 **Antigen Purification**

317 A variety of recombinant soluble protein antigens were used in the LIBRA-seq experiment and
318 other experimental assays.

319 Plasmids encoding residues 1–1208 of the SARS-CoV-2 spike with a mutated S1/S2
320 cleavage site, proline substitutions at positions 817, 892, 899, 942, 986 and 987, and a C-
321 terminal T4-fibrin trimerization motif, an 8x HisTag, and a TwinStrepTag (SARS-CoV-2 spike
322 HP); 1–1208 of the SARS-CoV-2 spike with a mutated S1/S2 cleavage site, proline substitutions
323 at positions 817, 892, 899, 942, 986 and 987, a glycine mutation at 614, and a C-terminal T4-
324 fibrin trimerization motif, an 8x HisTag, and a TwinStrepTag (SARS-CoV-2 spike HP D614G)
325 1–1208 of the SARS-CoV-2 spike with a mutated S1/S2 cleavage site, proline substitutions at
326 positions 817, 892, 899, 942, 986 and 987, as well as mutations L18F, D80A, L242-244L del,
327 R246I, K417N, E484K, N501Y, and a C-terminal T4-fibrin trimerization motif, an 8x HisTag,
328 and a TwinStrepTag (SARS-CoV-2 spike HP B.1.351); 1–1208 of the SARS-CoV-2 spike with a
329 mutated S1/S2 cleavage site, proline substitutions at positions 817, 892, 899, 942, 986 and 987,
330 as well as mutations 69-70del, Y144del, N501Y, A570D, P681H, and a C-terminal T4-fibrin
331 trimerization motif, an 8x HisTag, and a TwinStrepTag (SARS-CoV-2 spike HP B.1.1.7);
332 residues 1-1190 of the SARS-CoV spike with proline substitutions at positions 968 and 969, and
333 a C-terminal T4-fibrin trimerization motif, an 8x HisTag, and a TwinStrepTag (SARS-CoV S-

334 2P); residues 1-1291 of the MERS-CoV spike with a mutated S1/S2 cleavage site, proline
335 substitutions at positions 1060 and 1061, and a C-terminal T4-fibrin trimerization motif, an
336 AviTag, an 8x HisTag, and a TwinStrepTag (MERS-CoV S-2P Avi); residues 1-1278 of the
337 HCoV-OC43 spike with proline substitutions at positions 1070 and 1071, and a C-terminal T4-
338 fibrin trimerization motif, an 8x HisTag, and a TwinStrepTag (HCoV-OC43 S-2P); residues
339 319–591 of SARS-CoV-2 S with a C-terminal monomeric human IgG Fc-tag and an 8x HisTag
340 (SARS-CoV-2 RBD-SD1); residues 367–589 of MERS-CoV S with a C-terminal monomeric
341 human IgG Fc-tag and an 8x HisTag (MERS-CoV RBD); residues 306–577 of MERS-CoV S
342 with a C-terminal monomeric human IgG Fc-tag and an 8x HisTag (SARS-CoV RBD-SD1) were
343 transiently transfected into FreeStyle293F cells (Thermo Fisher) using polyethylenimine. For all
344 antigens with the exception of SARS-CoV-2 S HP, cells were treated with 1 μ M kifunensine to
345 ensure uniform glycosylation three hours post-transfection. Transfected supernatants were
346 harvested after 6 days of expression. SARS-CoV-2 RBD-SD1 was purified using Protein A resin
347 (Pierce), SARS-CoV-2 S HP, MERS-CoV S-2P, and HCoV-OC43 S-2P were purified using
348 StrepTactin resin (IBA). Affinity-purified SARS-CoV-2 RBD-SD1 was further purified over a
349 Superdex75 column (GE Life Sciences). SARS-CoV-2 S HP, SARS-CoV-2 S HP B.1.351,
350 SARS-CoV-2spikeHP B.1.1.7, SARS-CoV S-2P, MERS-CoV S-2P, HCoV-HKU1 S-2P and
351 HCoV-OC43 S-2P were purified over a Superose6 Increase column (GE Life Sciences). HCoV-
352 NL63 and HCoV-229E alpha coronavirus spike proteins were purchased from Sino Biological.
353 SARS-CoV-2 S1, SARS-CoV-2 S2, and SARS-CoV-2 NTD truncated proteins were purchased
354 from the commercial vendor, Sino Biological.

355 For the HIV-1 gp140 SOSIP variant from strain ZM197 (clade C) recombinant, soluble
356 antigens contained an AviTag and were expressed in Expi293F cells using polyethylenimine
357 transfection reagent and cultured. FreeStyle F17 expression medium supplemented with
358 pluronic acid and glutamine was used. The cells were cultured at 37°C with 8% CO₂ saturation

359 and shaking. After 5-7 days, cultures were centrifuged and supernatant was filtered and run
360 over an affinity column of agarose bound *Galanthus nivalis* lectin. The column was washed with
361 PBS and antigens were eluted with 30 mL of 1M methyl- α -D-mannopyranoside. Protein elutions
362 were buffer exchanged into PBS, concentrated, and run on a Superdex 200 Increase 10/300 GL
363 Sizing column on the AKTA FPLC system. Fractions corresponding to correctly folded protein
364 were collected, analyzed by SDS-PAGE and antigenicity was characterized by ELISA using
365 known monoclonal antibodies specific to each antigen. Avitagged antigens were biotinylated
366 using BirA biotin ligase (Avidity LLC).

367 Recombinant NC99 HA protein consists of the HA ectodomain with a point mutation at
368 the sialic acid-binding site (Y98F) to abolish non-specific interactions, a T4 fibrin foldon
369 trimerization domain, AviTag, and hexahistidine-tag, and were expressed in Expi 293F
370 mammalian cells using Expifectamine 293 transfection reagent (Thermo Fisher Scientific)
371 cultured for 4-5 days. Culture supernatant was harvested and cleared as above, and then
372 adjusted pH and NaCl concentration by adding 1M Tris-HCl (pH 7.5) and 5M NaCl to 50 mM
373 and 500 mM, respectively. Ni Sepharose excel resin (GE Healthcare) was added to the
374 supernatant to capture hexahistidine tag. Resin was separated on a column by gravity and
375 captured HA protein was eluted by a Tris-NaCl (pH 7.5) buffer containing 300 mM imidazole.
376 The eluate was further purified by a size exclusion chromatography with a HiLoad 16/60
377 Superdex 200 column (GE Healthcare). Fractions containing HA were concentrated, analyzed
378 by SDS-PAGE and tested for antigenicity by ELISA with known antibodies.

379 Spike protein used for cryo-EM was expressed by transiently transfecting plasmid
380 encoding the HexaPro spike variant (Hsieh et al., 2020) containing additional S383C and
381 D985C substitutions (Henderson et al., 2020) with a C-terminal TwinStrep tag into FreeStyle
382 293-F cells (Thermo Fisher) using polyethyleneimine. 5 μ M kifunensine was added 3h post-
383 transfection. The cell culture was harvested four days after transfection and the spike-containing

384 medium was separated from the cells by centrifugation. Supernatants were passed through a
385 0.22 µm filter and passaged over StrepTactin resin (IBA). Further purification was achieved by
386 size-exclusion chromatography using a Superose 6 10/300 column (GE Healthcare) in buffer
387 containing 2 mM Tris pH 8.0, 200 mM NaCl and 0.02% NaN₃.

388

389 **DNA-barcoding of Antigens**

390 We used oligos that possess 15 bp antigen barcode, a sequence capable of annealing to the
391 template switch oligo that is part of the 10X bead-delivered oligos, and contain truncated
392 TruSeq small RNA read 1 sequences in the following structure: 5'-
393 CCTTGGCACCCGAGAATTCCANNNNNNNNNNNNNNCCCATATAAGA*A*A-3', where Ns
394 represent the antigen barcode. We used the following antigen barcodes: We used the following
395 antigen barcodes: GCAGCGTATAAGTCA (SARS-CoV-2 S), AACCCACCGTTGTTA (SARS-
396 CoV-2 S D614G), GCTCCTTTACACGTA (SARS-CoV S), GGTAGCCCTAGAGTA (MERS-CoV
397 S), AGACTAATAGCTGAC (HCoV-OC43 S), GACAAGTGATCTGCA (HCoV-NL63 S),
398 GTGTGTTGTCCTATG (HCoV-229E S), TACGCCTATAACTTG (ZM197 EnV),
399 TCATTTCTCCGATT (HA NC99), TGGTAACGACAGTCC (SARS-CoV RBD-SD1),
400 TTTCAACGCCCTTTC (SARS-CoV-2 RBD-SD1), GTAAGACGCCTATGC (MERS-CoV RBD),
401 CAGTAAGTTCGGGAC(SARS-CoV-2 NTD), Oligos were ordered from IDT with a 5' amino
402 modification and HPLC purified.

403 For each antigen, a unique DNA barcode was directly conjugated to the antigen itself. In
404 particular, 5' amino-oligonucleotides were conjugated directly to each antigen using the Solulink
405 Protein-Oligonucleotide Conjugation Kit (TriLink cat no. S-9011) according to manufacturer's
406 instructions. Briefly, the oligo and protein were desalted, and then the amino-oligo was modified
407 with the 4FB crosslinker, and the biotinylated antigen protein was modified with S-HyNic. Then,

408 the 4FB-oligo and the HyNic-antigen were mixed together. This causes a stable bond to form
409 between the protein and the oligonucleotide. The concentration of the antigen-oligo conjugates
410 was determined by a BCA assay, and the HyNic molar substitution ratio of the antigen-oligo
411 conjugates was analyzed using the NanoDrop according to the Solulink protocol guidelines.
412 AKTA FPLC was used to remove excess oligonucleotide from the protein-oligo conjugates,
413 which were also verified using SDS-PAGE with a silver stain. Antigen-oligo conjugates were
414 also used in flow cytometry titration experiments.

415

416 **Antigen-specific B cell sorting**

417 Cells were stained and mixed with DNA-barcoded antigens and other antibodies, and then
418 sorted using fluorescence activated cell sorting (FACS). First, cells were counted and viability
419 was assessed using Trypan Blue. Then, cells were washed three times with DPBS
420 supplemented with 0.1% Bovine serum albumin (BSA). Cells were resuspended in DPBS-BSA
421 and stained with cell markers including viability dye (Ghost Red 780), CD14-APC-Cy7, CD3-
422 FITC, CD19-BV711, and IgG-PE-Cy5. Additionally, antigen-oligo conjugates were added to the
423 stain. After staining in the dark for 30 minutes at room temperature, cells were washed three
424 times with DPBS-BSA at 300 g for five minutes. Cells were then incubated for 15 minutes at
425 room temperature with Streptavidin-PE to label cells with bound antigen. Cells were washed
426 three times with DPBS-BSA, resuspended in DPBS, and sorted by FACS. Antigen positive cells
427 were bulk sorted and delivered to the Vanderbilt Technologies for Advanced Genomics
428 (VANTAGE) sequencing core at an appropriate target concentration for 10X Genomics library
429 preparation and subsequent sequencing. FACS data were analyzed using FlowJo.

430

431 **Sample preparation, library preparation, and sequencing**

432 Single-cell suspensions were loaded onto the Chromium Controller microfluidics device (10X
433 Genomics) and processed using the B-cell Single Cell V(D)J solution according to
434 manufacturer's suggestions for a target capture of 10,000 B cells per 1/8 10X cassette, with
435 minor modifications in order to intercept, amplify and purify the antigen barcode libraries as
436 previously described (Setliff et al., 2019).

437

438 **Sequence processing and bioinformatics analysis**

439 We utilized and modified our previously described pipeline to use paired-end FASTQ files of
440 oligo libraries as input, process and annotate reads for cell barcode, unique molecular identifier
441 (UMI), and antigen barcode, and generate a cell barcode - antigen barcode UMI count matrix
442 (Setliff et al., 2019). BCR contigs were processed using Cell Ranger (10X Genomics) using
443 GRCh38 as reference. Antigen barcode libraries were also processed using Cell Ranger (10X
444 Genomics). The overlapping cell barcodes between the two libraries were used as the basis of
445 the subsequent analysis. We removed cell barcodes that had only non-functional heavy chain
446 sequences as well as cells with multiple functional heavy chain sequences and/or multiple
447 functional light chain sequences, reasoning that these may be multiplets. Additionally, we
448 aligned the BCR contigs (filtered_contigs.fasta file output by Cell Ranger, 10X Genomics) to
449 IMGT reference genes using HighV-Quest (Alamyar et al., 2012). The output of HighV-Quest
450 was parsed using ChangeO(Gupta et al., 2015) and merged with an antigen barcode UMI count
451 matrix. Finally, we determined the LIBRA-seq score for each antigen in the library for every cell
452 as previously described(Setliff et al., 2019).

453

454 **Antibody expression and purification**

455 For each antibody, variable genes were inserted into custom plasmids encoding the constant
456 region for the IgG1 heavy chain as well as respective lambda and kappa light chains (pTwist
457 CMV BetaGlobin WPRE Neo vector, Twist Bioscience). Antibodies were expressed in Expi293F
458 mammalian cells (Thermo Fisher Scientific) by co-transfecting heavy chain and light chain
459 expressing plasmids using polyethylenimine transfection reagent and cultured for 5-7 days.
460 Cells were maintained in FreeStyle F17 expression medium supplemented at final
461 concentrations of 0.1% Pluronic Acid F-68 and 20% 4mM L-Glutamine. These cells were
462 cultured at 37°C with 8% CO₂ saturation and shaking. After transfection and 5-7 days of culture,
463 cell cultures were centrifuged and supernatant was 0.45 µm filtered with Nalgene Rapid Flow
464 Disposable Filter Units with PES membrane. Filtered supernatant was run over a column
465 containing Protein A agarose resin equilibrated with PBS. The column was washed with PBS,
466 and then antibodies were eluted with 100 mM Glycine HCl at 2.7 pH directly into a 1:10 volume
467 of 1M Tris-HCl pH 8.0. Eluted antibodies were buffer exchanged into PBS 3 times using Amicon
468 Ultra centrifugal filter units and concentrated. Antibodies were analyzed by SDS-PAGE.

469

470 **High-throughput antibody expression**

471 For high-throughput production of recombinant antibodies, approaches were used that are
472 designated as microscale. For antibody expression, microscale transfection were performed
473 (~1 ml per antibody) of CHO cell cultures using the Gibco ExpiCHO Expression System and a
474 protocol for deep 96-well blocks (Thermo Fisher Scientific). In brief, synthesized antibody-
475 encoding DNA (~2 µg per transfection) was added to OptiPro serum free medium (OptiPro
476 SFM), incubated with ExpiFectamine CHO Reagent and added to 800 µl of ExpiCHO cell
477 cultures into 96-deep-well blocks using a ViaFlo 384 liquid handler (Integra Biosciences). The
478 plates were incubated on an orbital shaker at 1,000 r.p.m. with an orbital diameter of 3 mm at
479 37 °C in 8% CO₂. The next day after transfection, ExpiFectamine CHO Enhancer and ExpiCHO

480 Feed reagents (Thermo Fisher Scientific) were added to the cells, followed by 4 d incubation for
481 a total of 5 d at 37 °C in 8% CO₂. Culture supernatants were collected after centrifuging the
482 blocks at 450g for 5 min and were stored at 4°C until use. For high-throughput microscale
483 antibody purification, fritted deep-well plates were used containing 25 µl of settled protein G
484 resin (GE Healthcare Life Sciences) per well. Clarified culture supernatants were incubated with
485 protein G resin for antibody capturing, washed with PBS using a 96-well plate manifold base
486 (Qiagen) connected to the vacuum and eluted into 96-well PCR plates using 86 µl of 0.1 M
487 glycine-HCL buffer pH 2.7. After neutralization with 14 µl of 1 M Tris-HCl pH 8.0, purified
488 antibodies were buffer-exchanged into PBS using Zeba Spin Desalting Plates (Thermo Fisher
489 Scientific) and stored at 4°C until use.

490

491 **ELISA**

492 To assess antibody binding, soluble protein was plated at 2 µg/ml overnight at 4°C. The next
493 day, plates were washed three times with PBS supplemented with 0.05% Tween-20 (PBS-T)
494 and coated with 5% milk powder in PBS-T. Plates were incubated for one hour at room
495 temperature and then washed three times with PBS-T. Primary antibodies were diluted in 1%
496 milk in PBS-T, starting at 10 µg/ml with a serial 1:5 dilution and then added to the plate. The
497 plates were incubated at room temperature for one hour and then washed three times in PBS-T.
498 The secondary antibody, goat anti-human IgG conjugated to peroxidase, was added at 1:10,000
499 dilution in 1% milk in PBS-T to the plates, which were incubated for one hour at room
500 temperature. Plates were washed three times with PBS-T and then developed by adding
501 3,3',5,5'-tetramethylbenzidine (TMB) substrate to each well. The plates were incubated at room
502 temperature for ten minutes, and then 1N sulfuric acid was added to stop the reaction. Plates
503 were read at 450 nm. Data are represented as mean ± SEM for one ELISA experiment. ELISAs

504 were repeated 2 or more times. The area under the curve (AUC) was calculated using
505 GraphPad Prism 9.0.1.

506

507 **Competition ELISA**

508 Competition ELISA was performed as done previously (Zost et al., 2020). Briefly, antibodies
509 were biotinylated using NHS-PEG4-biotin (Thermo Fisher Scientific, cat# A39259) according to
510 manufacturer protocol. Following biotinylation, specific binding of biotinylated antibodies was
511 confirmed using ELISA. Wells of 384-well microtiter plates were coated with 1 µg/mL SARS-
512 CoV-2 S HP protein at 4°C overnight. Plates were washed with PBS-T and blocked for 1 h with
513 blocking buffer (1% BSA in PBS-T). Plates were then washed with PBS-T and unlabeled
514 antibodies were added at a concentration of 10 µg/mL in a total volume of 25 µL blocking buffer
515 and incubated 1 h. Without washing, biotinylated antibodies diluted in blocking buffer were
516 added directly to each well in a volume of 5 µL per well (such that the final concentrations of
517 each biotinylated antibody were equal to the respective EC₉₀ of each antibody), and then
518 incubated for 30 min at ambient temperature. Plates were then washed with PBS-T and
519 incubated for 1 h with HRP-conjugated avidin (Sigma, 25 µL of a 1:3,500 dilution in blocking
520 buffer). Plates were washed with PBS-T and 25 µL TMB substrate was added to each well. After
521 sufficient development, the reactions were quenched by addition 25 µL 1M HCl and absorbance
522 at 450 nm was quantified using a plate reader. After subtracting the background signal, the
523 signal obtained for binding of the biotin-labeled reference antibody in the presence of the
524 unlabeled tested antibody was expressed as a percentage of the binding of the reference
525 antibody in the presence of 10 µg/mL of the anti-dengue antibody DENV 2D22, which served as
526 a no-competition control. Tested antibodies were considered competing if their presence
527 reduced the reference antibody binding by more than 60% and non-competing if the signal was
528 reduced by less than 30%.

529

530 **Real-time Cell Analysis (RTCA) Neutralization Assay Screen**

531 To screen for neutralizing activity in the panel of recombinantly expressed antibodies, we used a
532 high-throughput and quantitative RTCA assay and xCelligence RTCA HT Analyzer (ACEA
533 Biosciences) that assesses kinetic changes in cell physiology, including virus-induced
534 cytopathic effect (CPE). Twenty μ l of cell culture medium (DMEM supplemented with 2% FBS)
535 was added to each well of a 384-well E-plate using a ViaFlo384 liquid handler (Integra
536 Biosciences) to obtain background reading. Six thousand (6,000) Vero-furin cells in 20 μ l of cell
537 culture medium were seeded per well, and the plate was placed on the analyzer. Sensograms
538 were visualized using RTCA HT software version 1.0.1 (ACEA Biosciences). For a screening
539 neutralization assay, equal amounts of virus were mixed with micro-scale purified antibodies in
540 a total volume of 40 μ L using DMEM supplemented with 2% FBS as a diluent and incubated for
541 1 h at 37 °C in 5% CO₂. At ~17–20 h after seeding the cells, the virus–antibody mixtures were
542 added to the cells in 384-well E-plates. Wells containing virus only (in the absence of antibody)
543 and wells containing only Vero cells in medium were included as controls. Plates were
544 measured every 8–12 h for 48–72 h to assess virus neutralization. Micro-scale antibodies were
545 assessed in four 5-fold dilutions (starting from a 1:20 sample dilution), and their concentrations
546 were not normalized. Neutralization was calculated as the percent of maximal cell index in
547 control wells without virus minus cell index in control (virus-only) wells that exhibited maximal
548 CPE at 40–48 h after applying virus–antibody mixture to the cells. An antibody was classified as
549 fully neutralizing if it completely inhibited SARS-CoV-2-induced CPE at the highest tested
550 concentration, while an antibody was classified as partially neutralizing if it delayed but did not
551 fully prevent CPE at the highest tested concentration (Zost et al., 2020)).

552

553 **RTCA Potency Neutralization Screening Assay**

554 To determine neutralizing activity of IgG, we used real-time cell analysis (RTCA) assay on an
555 xCELLigence RTCA MP Analyzer (ACEA Biosciences Inc.) that measures virus-
556 induced cytopathic effect (CPE) (Suryadevara N et al., 2021). Briefly, 50 μ L of cell culture
557 medium (DMEM supplemented with 2% FBS) was added to each well of a 96-well E-plate using
558 a ViaFlo384 liquid handler (Integra Biosciences) to obtain background reading. A suspension of
559 18,000 Vero-E6 cells in 50 μ L of cell culture medium was seeded in each well, and the plate
560 was placed on the analyzer. Measurements were taken automatically every 15 min, and the
561 sensograms were visualized using RTCA software version 2.1.0 (ACEA Biosciences Inc). VSV-
562 SARS-CoV-2 (0.01 MOI, ~120 PFU per well) was mixed 1:1 with a dilution of antibody in a total
563 volume of 100 μ L using DMEM supplemented with 2% FBS as a diluent and incubated for 1 h at
564 37°C in 5% CO₂. At 16 h after seeding the cells, the virus-antibody mixtures were added in
565 replicates to the cells in 96-well E-plates. Triplicate wells containing virus only (maximal CPE in
566 the absence of antibody) and wells containing only Vero cells in medium (no-CPE wells) were
567 included as controls. Plates were measured continuously (every 15 min) for 48 h to assess virus
568 neutralization. Normalized cellular index (CI) values at the endpoint (48 h after incubation with
569 the virus) were determined using the RTCA software version 2.1.0 (ACEA Biosciences Inc.).
570 Results are expressed as percent neutralization in a presence of respective antibody relative to
571 control wells with no CPE minus CI values from control wells with maximum CPE. RTCA
572 IC₅₀ values were determined by nonlinear regression analysis using Prism software.

573

574 **Epitope mapping of antibodies by alanine scanning**

575 Epitope mapping was performed essentially as described previously (Davidson, 2014) using a SARS-
576 CoV-2 (strain Wuhan-Hu-1) spike protein RBD shotgun mutagenesis mutation library, made using an
577 expression construct for full-length spike protein. 184 residues of the RBD (between spike residues

578 335 and 526) were mutated individually to alanine, and alanine residues to serine and clones arrayed
579 in 384-well plates, one mutant per well. Antibody binding to each mutant clone was determined, in
580 duplicate, by high-throughput flow cytometry. Each spike protein mutant was transfected into HEK-
581 293T cells and allowed to express for 22 hrs. Cells were fixed in 4% (v/v) paraformaldehyde (Electron
582 Microscopy Sciences), and permeabilized with 0.1% (w/v) saponin (Sigma-Aldrich) in PBS plus
583 calcium and magnesium (PBS++) before incubation with antibodies diluted in PBS++, 10% normal
584 goat serum (Sigma), and 0.1% saponin. Antibody screening concentrations were determined using
585 an independent immunofluorescence titration curve against cells expressing wild-type spike protein
586 to ensure that signals were within the linear range of detection. Antibodies were detected using 3.75
587 $\mu\text{g/mL}$ of AlexaFluor488-conjugated secondary antibody (Jackson ImmunoResearch Laboratories) in
588 10% normal goat serum with 0.1% saponin. Cells were washed three times with PBS++/0.1% saponin
589 followed by two washes in PBS, and mean cellular fluorescence was detected using a high-
590 throughput Intellicyte iQue flow cytometer (Sartorius). Antibody reactivity against each mutant spike
591 protein clone was calculated relative to wild-type spike protein reactivity by subtracting the signal from
592 mock-transfected controls and normalizing to the signal from wild-type S-transfected controls.
593 Mutations within clones were identified as critical to antibody binding if they did not support reactivity
594 of the test antibody, but supported reactivity of other SARS-CoV-2 antibodies. This counter-screen
595 strategy facilitates the exclusion of spike mutants that are locally misfolded or have an expression
596 defect.

597

598 **Plaque reduction neutralization test (PRNT)**

599 The virus neutralization with live authentic SARS-CoV-2 virus (USA-WA1) was performed in the
600 BSL-3 facility of the Galveston National Laboratory using Vero E6 cells (ATCC CRL-1586)
601 following the standard procedure. Briefly, Vero E6 cells were cultured in 96-well plates (10^4
602 cells/well). Next day, 4-fold serial dilutions of antibodies were made using MEM-2% FBS, as to

603 get an initial concentration of 100 µg/ml. Equal volume of diluted antibodies (60 µl) were mixed
604 gently with original SARS-CoV-2 or B.1.1.7 variant or B.1.351 variant (60 µl containing 200 pfu)
605 and incubated for 1 h at 37°C/5% CO₂ atmosphere. The virus-serum mixture (100 µl) was
606 added to cell monolayer in duplicates and incubated for 1 at h 37°C/5% CO₂ atmosphere. Later,
607 virus-serum mixture was discarded gently, and cell monolayer was overlaid with 0.6%
608 methylcellulose and incubated for 2 days. The overlay was removed, and the plates were fixed
609 in 4% paraformaldehyde twice following BSL-3 protocol. The plates were stained with 1%
610 crystal violet and virus-induced plaques were counted. The percent neutralization and/or NT₅₀ of
611 antibody was calculated by dividing the plaques counted at each dilution with plaques of virus-
612 only control. For antibodies, the inhibitory concentration at 50% (IC₅₀) values were calculated in
613 GraphPad Prism software by plotting the midway point between the upper and lower plateaus of
614 the neutralization curve among dilutions.

615

616 **BioLayer Interferometry (BLI)**

617 Purified 54042-4 IgG was immobilized to AHC sensortips (FortéBio) to a response level of
618 approximately 1.4 nm in a buffer composed of 10 mM HEPES pH 7.5, 150 mM NaCl, 3 mM
619 EDTA, 0.05% Tween 20 and 0.1% (w/v) BSA. Immobilized IgG was then dipped into wells
620 containing four-fold dilutions of SARS-CoV-2 RBD-SD1 ranging in concentration from 100-
621 1.5625 nM, to measure association. Dissociation was measured by dipping sensortips into wells
622 containing only running buffer. Data were reference subtracted and kinetics were calculated in
623 Octet Data Analysis software v10.0 using a 1:1 binding model.

624

625 **ACE2 binding inhibition assay**

626 96-well plates were coated with 2 µg/mL purified recombinant SARS-CoV-2 at 4°C overnight.
627 The next day, plates were washed three times with PBS supplemented with 0.05% Tween-20
628 (PBS-T) and coated with 5% milk powder in PBS-T. Plates were incubated for one hour at room
629 temperature and then washed three times with PBS-T. Purified antibodies were diluted in
630 blocking buffer at 10 µg/mL in triplicate, added to the wells, and incubated at room temperature.
631 Without washing, recombinant human ACE2 protein with a mouse Fc tag was added to wells for
632 a final 0.4 µg/mL concentration of ACE2 and incubated for 40 minutes at room temperature.
633 Plates were washed three times with PBS-T, and bound ACE2 was detected using HRP-
634 conjugated anti-mouse Fc antibody and TMB substrate. The plates were incubated at room
635 temperature for ten minutes, and then 1N sulfuric acid was added to stop the reaction. Plates
636 were read at 450 nm. ACE2 binding without antibody served as a control. Experiment was done
637 in biological replicate and technical triplicates.

638

639 **Neutralization escape**

640 We used a real-time cell analysis assay (RTCA) and xCELLigence RTCA MP Analyzer (ACEA
641 Biosciences Inc.) with modification of previously described assays (Gilchuk et al.,
642 2020a; Weisblum et al., 2020, Suryadevara et al.,2021). Fifty (50) µL of cell culture medium
643 (DMEM supplemented with 2% FBS) was added to each well of a 96-well E-plate to obtain a
644 background reading. Eighteen thousand (18,000) Vero E6 cells in 50 µL of cell culture medium
645 were seeded per each well, and plates were placed on the analyzer. Measurements were taken
646 automatically every 15 min and the sensograms were visualized using RTCA software version
647 2.1.0 (ACEA Biosciences Inc). COV2-2130 or COV2-2499 or WT VSV-SARS-CoV-2 virus (5e3
648 plaque forming units [PFU] per well, ~0.3 MOI) was mixed with a saturating neutralizing
649 concentration of individual antibody (5 µg/mL) in a total volume of 100 µL and incubated for 1 h
650 at 37°C. At 16-20 h after seeding the cells, the virus-antibody mixtures were added into 8 to 96

651 replicate wells of 96-well E-plates with cell monolayers. Wells containing only virus in the
652 absence of antibody and wells containing only Vero E6 cells in medium were included on each
653 plate as controls. Plates were measured continuously (every 15 min) for 72 h. The escapes from
654 54042-4 was confirmed by delayed CPE in wells containing antibody while mAb2381 was used
655 as positive control.

656

657 **EM sample prep and data collection**

658 To form the spike-Fab complex, a final concentration of 0.5 mg/mL spike protein and 5X molar
659 excess of Fab were combined in buffer containing 2mM Tris-Cl pH 8.0, 200 mM NaCl, and
660 0.02% NaN₃. The complex was incubated on ice for 30 min before 3 μ L of the sample was
661 deposited on Au-300 1.2/1.3 grids (UltrAuFoil) that had been plasma cleaned in a Solarus 950
662 plasma cleaner (Gatan) for 4 minutes using a 4:1 ratio of O₂:H₂. A force of -4 was used to blot
663 excess liquid for 3 s using a Vitrobot Mark IV (Thermo Fisher) followed by plunge-freezing with
664 liquid ethane. 3,762 micrographs were collected from a single grid using a Titan Krios (Thermo
665 Fisher) equipped with a K3 detector (Gatan) with the stage set at a 30° tilt. SerialEM was used
666 to collect movies at 29,000X nominal magnification with a calibrated pixel size of 0.81 Å/pixel.
667 Additional details about data collection parameters can be found in **Supplemental Table 1**.

668

669 **Cryogenic electron microscopy (Cryo-EM)**

670 Motion correction, CTF estimation, particle picking, and preliminary 2D classification were
671 performed using cryoSPARC v3.2.0 live processing (Punjani et al., 2017). The final iteration of
672 2D class averaging distributed 374,669 particles into 60 classes using an uncertainty factor of 2.
673 From that, 241,732 particles were used to perform an ab initio reconstruction with four classes
674 followed by heterogeneous refinement of those four classes. Particles from the two highest

675 quality classes were used for homogenous refinement of the best volume with applied C3
676 symmetry. Non-uniform refinement was performed on the resulting volume using per-particle
677 defocus and per-group CTF optimizations applied (Punjani et al., 2020; Rubinstein and
678 Brubaker, 2015). To improve the 54042-4 Fab-RBD density, C3 symmetry expansion was
679 performed followed by local refinement using a mask created in ChimeraX that encompassed
680 the entire 54042-4 Fab and RBD (Pettersen et al., 2021). Local refinement was performed using
681 a pose/shift gaussian prior during alignment, 3° standard deviation of prior over rotation and 1 Å
682 standard deviation of prior over shifts. Additionally, maximum alignment resolution was limited to
683 2.8 Å resolution to avoid over-refining. To improve map quality, the focused refinement volumes
684 were processed using the DeepEMhancer(Sanchez-Garcia, 2021) tool via COSMIC²science
685 gateway, which included the use of our refinement mask to help define noise while sharpening
686 (Cianfrocco, 2017a; Cianfrocco, 2017b). An initial model was generated by docking PDBID:
687 6XKL (Hsieh et al., 2020) and a Fab model based on the 54042-4 sequence built using
688 SAbPred ABodyBuilder (Dunbar et al., 2016) into map density via ChimeraX (Pettersen et al.,
689 2021). The model was iteratively refined and completed using a combination of Phenix, Coot,
690 and ISOLDE (Adams et al., 2002; Croll, 2018; Emsley and Cowtan, 2004). Details on structure
691 validation and the full cryo-EM processing workflow can be found in **Supplemental Figures 5**
692 **and 6**.

693

694 **GISAID mutation frequency calculation**

695 To evaluate the conservation of 54042-4 epitope residues, we utilized the GISAID database
696 (Elbe, 2017) comprising sequences from 1229459 SARS-CoV-2 variants (as of May 6th, 2021).
697 The spike glycoprotein sequences were extracted and translated, and pairwise sequence
698 alignment with the reference sequence hCoV-19/Wuhan/WIV04/2019 was then performed. After
699 removing incomplete sequences and sequences with alignment errors, the pairwise alignments

700 for the remaining 1,148,887 spike protein sequences were combined to compute the
701 conservation of each residue position using in-house perl scripts.

702

703 **RMSD calculation for the differences in angle of antigen approach for different antibodies**

704 The SARS-CoV-2 spike receptor binding domain coordinates present in each antibody-antigen
705 complex were aligned in PyMOL (The PyMOL Molecular Graphics System, Version 1.2r3pre,
706 Schrödinger, LLC.) using an all-atom alignment with 5 cycles of outlier rejection of atom pairs
707 having an RMSD greater than 2. The alignment was performed for RBD residues 329-529 in
708 antibody 54042-4 (PDB ID: TBD chain A), 329-529 in antibody 2-7 (PDB ID: 7LSS chain B), and
709 333-526 in antibody REGN10987 (PDB ID: 6XDG chain A). This resulted in RMSD values of
710 0.751 Å between 54042-4 and REGN10987's RBDs, 1.044 Å between 54042-4 and antibody 2-
711 7's RBDs, and 1.067 Å between REGN10987 and antibody 2-7's RBDs with well-aligned
712 epitope residues. Next, the residues comprising the N-termini through the end of framework
713 region 3 were determined for the heavy and light chains of all three antibodies using IMGT
714 Domain Gap Align (Alamyar et al., 2012). Each pair of antibodies was aligned using a pairwise
715 sequence alignment of this region in PyMOL. Finally, the alpha carbon root mean square
716 deviation between antibodies was calculated over this region in the heavy and light chains using
717 residue pairs from the sequence alignment. RMSD values were calculated from 183, 183, and
718 180 alpha carbon pairs for the 54042-4 vs REGN1087, REGN1087 vs 2-7, and 54042-4 vs 2-7
719 comparisons respectively.

720

721 **QUANTIFICATION AND STATISTICAL ANALYSIS**

722 ELISA error bars (standard error of the mean) were calculated using GraphPad Prism version
723 9.0.1.

725 **FIGURE CAPTIONS**

726 **Figure 1. Identification and characterization of SARS-CoV-2 antibodies isolated using**
727 **LIBRA-seq**

728 **(A)** Variable heavy gene usage (x-axis) as a function of IgG⁺ B cells with a SARS-CoV-2 spike
729 LIBRA-seq score (>1) (y-axis). The nine lead candidates are highlighted in purple.

730 **(B)** RTCA VSV-SARS-CoV-2 neutralization by lead candidate antibodies. IC₅₀ values are
731 calculated by non-linear regression analysis by GraphPad Prism software.

732 **(C)** Sequence characteristics and antigen specificity of nine lead candidate antibodies from a
733 recovered COVID-19 donor. Percent identity is calculated at the nucleotide level, and CDR
734 length and sequences are displayed at the amino acid level. LIBRA-seq scores for each
735 antigen are displayed as a heatmap with a LIBRA-seq score of -2 displayed as light yellow,
736 0 as white, and 2 in purple; in this heatmap scores lower or higher than that range are
737 shown as -2 and 2, respectively. ELISA binding data for SARS-CoV-2 S are displayed as a
738 heatmap of the AUC analysis calculated from (**Supplemental Figure 1C**) with AUC of 0
739 displayed as light yellow, 50% maximum as white, and maximum AUC as purple.

740

741 **Figure 2: 54042-4 functional characterization**

742 **(A)** ELISA binding values against SARS-CoV-2 subdomains are displayed as a heatmap of
743 AUC values calculated from the data in (**Supplemental Figure 2**). Antibodies CR3022,
744 46472-6, 46472-4 were used as positive controls for the RBD, NTD, and S2 antigens,
745 respectively (Shiakolas et al., 2020; Yuan et al., 2020b). 3602-1707 was included as an
746 influenza HA-specific negative control antibody (Setliff et al., 2019).

747 **(B)** A biolayer interferometry sensogram that shows binding to recombinant SARS-CoV-2 RBD-
748 SD1. Binding data are depicted by the black lines and the best fit line of the data to a 1:1
749 binding model is shown in red.

750 **(C)** SARS-CoV-2 spike/ACE2 inhibition ELISA is shown, for 54042-4, SARS-CoV-2 antibody
751 CR3022 and negative control HA-specific antibody 3602-1707. For each antibody, the ACE2
752 binding signal is depicted on the y-axis, in comparison to ACE2-only binding to SARS-COV-
753 2 spike shown as a dotted line.

754 **(D)** Competition ELISA of 54042-4 with antibodies COV2-2196, COV2-2130, and CR3022.
755 Values in white indicate no competition (presence of competing antibody reduced reference
756 antibody binding by less than 30%) and values in dark grey indicate competition (presence
757 of competing antibody reduced reference antibody binding by more than 60%).

758

759 **Figure 3: Atomic resolution of 54042-4 binding mode to SARS-CoV-2 S**

760 **(A)** 3D reconstructions of side and top views of Fab 54042-4 bound to SARS-CoV-2 spike.
761 **(B)** Focused refinement maps showing the 54042-4 epitope at the apex of the RBM in the down
762 position (left). Top-down view of the 54042-4 epitope showing heavy and light chain
763 contacts, as well as residues outside of the binding interface that are mutated in circulating
764 VOCs (right).

765 **(C)** The 54042-4 heavy chain binds to RBD residues 443–447 primarily through a network of
766 hydrogen bonds involving CDRH2 and CDRH3 and hydrophobic contacts involving Ile32 of
767 CRDH1.

768 **(D)** The 54042-4 light chain contacts RBD residues 498–500 through a hydrogen bond between
769 Thr500 and His92 of CDRL3 and hydrophobic contacts involving Phe30 and Tyr32 of
770 CDRL1.

771

772 **Figure 4: Sequence and structural comparison of 54042-4 to known SARS-CoV-2**
773 **antibodies**

774 **(A)** Amino acid CDRH3 identity to 54042-4 (x-axis) is plotted against CDRL3 identity to 54042-4
775 (y-axis) for paired heavy and light chain sequences obtained from the CoV-AbDab
776 database. Antibodies using the same heavy and light chain germline gene as 54042-
777 4 (*IGHV2-5* and *IGKV1-39*) are shown in light blue. Antibodies using the *IGHV2-5* heavy
778 chain gene and a non-*IGKV1-39* light chain gene are shown in orange. Additionally,
779 antibodies using a non-*IGHV2-5* heavy chain gene and the *IGKV1-39* light chain gene, with
780 CDRH3 or CDRL3 identity to 54042-4 of at least 50%, are highlighted in purple. Finally,
781 antibodies that do not use *IGHV2-5* or *IGKV1-39*, but that have at least 50% identity to
782 CDRH3 or CDRL3 of 54042-4, are shown in grey.

783
784 **(B)** Pearson correlation of epitopes of known SARS-CoV-2 antibodies in comparison to 54042-4
785 antibody, with the four antibodies showing a statistically significant ($p < 0.05$) positive
786 correlation highlighted in red.

787 **(C)** Heatmap (top) depicting buried surface area (\AA^2) at the SARS-CoV-2 RBD interface for the
788 four antibodies with highest epitope correlations with 54042-4. Bar graph (bottom) showing
789 the frequency (%) of substitutions at each given residue position in log scale, with a dashed
790 line at 1% and residue positions with a frequency greater than 1% highlighted in red.

791 **(D)** Distinct angles of approach of antibodies 54042-4 (heavy chain: orange, light chain: white),
792 REGN10987 (heavy chain: blue, light chain: white) (PDB id: 6XDG), and 2-7 (heavy chain:
793 pink, light chain: white) (PDB id: 7LSS) to the SARS-CoV-2 RBD (green).

794 **(E)** Structural comparison of CDRH1, 2, and 3 of antibodies 54042-4 and 2-7. CDRH1 of 2-7
795 extends further than 54042-4, forming additional contacts with Thr345 and Arg346 of the
796 RBD (left). The CDRH2 region of 2-7 approaches at a different angle, but maintains RBD
797 contacts via Asp56 and Arg58 (center). The CDRH3 contacts of 2-7 and 54042-4 are
798 divergent, with unique CDRH3 residues and RBD interactions (right).

799

800 **Figure 5: Functional characterization of antibody 54042-4**

801 **(A)** Binding data of 54042-4 antibody to a shotgun alanine mutagenesis screening library of the
802 SARS-CoV-2 RBD (Wuhan-Hu-1 strain). Residues displayed are the alanine mutations that
803 resulted in the biggest loss of binding to 54042-4 yet still retained signal with the RBD
804 antibody control.

805 **(B)** RTCA Neutralization of VSV SARS-CoV-2 chimera variants harboring specific mutations.
806 Cell sensograms are shown in boxes corresponding to mutations indicated in each row.
807 Columns (from left to right) are each chimera treated with antibody2381 and 54042-4 and
808 virus only control. Neutralization of 54042-4 of USA-WA1 strain and cells only are indicated
809 on the right. COV2-2381 was chosen as a positive control due to its distinct epitope footprint
810 from the selected mutations.

811 **(C)** 54042-4 epitope residues (non-zero buried surface area on SARS-CoV-2 RBD) with their
812 associated % conservation (the percentage of deposited sequences containing the highest-
813 frequency amino acid at that position) in the GISAID database. The only 54042-4 epitope
814 residue with a % conservation of less than 99%, N439, is highlighted in red.

815 **(D)** ELISA AUC of 54042-4, CR3022, and an influenza HA-specific negative control antibody
816 3602-1707. AUC is displayed as a heatmap with a value of 0 corresponding to white, 50%
817 maximum as light-purple, and maximum AUC as purple.

818 **(E)** Authentic SARS-CoV-2 neutralization of USA-WA1, B.1.1.7, and B.1.351 is depicted as a
819 function of antibody concentration.

820

821

822

823 **Supplemental Figure 1**

824 **(A)** VSV-SARS-CoV-2 capacity of serum is displayed from time points at day 18, day 28, day
825 56, and days 80-90.

826 **(B)** Gating scheme for fluorescent-activated cell sorting of recovered COVID-19 individual. Cells
827 were stained with Ghost Red 780, CD14-APC-Cy7, CD3-FITC, CD19-BV711, and IgG-PE-
828 Cy5 along with a DNA-barcoded antigen screening library. To detect antigen-positive B
829 cells, cells were washed and treated with a streptavidin-PE secondary stain. Gates as drawn
830 are based on gates used during the sort, and percentages from the sort are listed.

831 **(C)** ELISA binding data of candidate antibodies identified by LIBRA-seq against SARS-CoV-2
832 spike HP.

833

834 **Supplemental Figure 2**

835 ELISA binding data against SARS-CoV-2 subdomains RBD, NTD, S1, and S2 are shown.
836 CR3022 was used as a positive control RBD-directed antibody(Yuan et al., 2020a) whereas
837 46472-4 and 46472-6 antibodies were used as positive controls for the S2 and NTD,
838 respectively (Shiakolas et al., 2020). The HA-specific 3602-1707 antibody was used as a
839 negative control.

840

841 **Supplemental Figure 3**

842 **(A)** SARS-CoV-2 spike residues comprising the epitope of 54042-4 are shown with their
843 associated buried surface area (\AA^2).

844 **(B)** 54042-4 residues comprising the antibody paratope against SARS-CoV-2 spike are shown
845 with their associated buried surface area values (\AA^2).

846

847 **Supplemental Figure 4**

848 **(A)** ELISA binding data against SARS-CoV-2 Wuhan-1 RBD and RBDs with substitutions
849 E484K, N501Y, N439K, or K417N. CR3022 was used as a positive control and 3602-1707,
850 an HA-specific antibody, was used as a negative control.

851 **(B)** ELISA binding data against SARS-CoV-2 S HP, SARS-CoV S, and SARS-CoV-2 S HP
852 constructs with substitutions in the S1 domain for the B.1.351, and B.1.1.7 variants of
853 concern. CR3022 was used as a positive control and 3602-1707 was used as a negative
854 control antibody.

855 **(C)** The substitutions and deletions present in the B.1.1.7 and B.1.351 constructs used in the
856 ELISAs depicted in **Supplemental Figure 4B**.

857

858 **Supplemental Figure 5: Cryo-EM data processing workflow.**

859 Flowchart outlining cryo-EM data processing of Fab 54042-4 Fab bound to SARS-CoV-2 S.
860 Additional information can be found in the Methods section under “Cryogenic electron
861 microscopy (cryo-EM)”.

862

863 **Supplemental Figure 6: Cryo-EM structure validation.**

864 **(A)** FSC curve and distribution plot for the C3 S-ECD/54042-4 structure, generated in
865 cryoSPARC v3.2.0.

866 **(B)** FSC curve and viewing distribution plot for focused refinement of the S-RBD bound to
867 54042-4 Fab.

868 **(C)** Local resolution shown by color of the C3 S-ECD/54042-4 (left) and focused S-RBD/54042-
869 4 (right) reconstructions.

870 **(D)** Map resulting from focused refinement of the RBD (green) (left), 54042-4 heavy chain
871 (orange), and 54042-4 light chain (white). Detailed views of the binding interface and

872 corresponding map (center, right). Oxygen atoms are colored red, nitrogen blue, and sulfur

873 yellow.

874

875

876 **Supplemental Table 1: PDB validation report**

EM data collection

Microscope	FEI Titan Krios
Voltage (kV)	300
Detector	Gatan K3
Magnification (nominal)	29,000
Pixel size (Å/pix)	0.81
Exposure rate (e ⁻ /pix/sec)	9.66
Frames per exposure	100
Exposure (e ⁻ /Å ²)	70
Defocus range (µm)	1.5-2.5
Tilt angle (°)	30
Micrographs collected	3,762
Micrographs used	1,610
Particles extracted (total)	516,664
Automation software	SerialEM
Sample	SARS-CoV-2 S + 54042-4 Fab

3D reconstruction statistics

	Overall	RBD-54042-4 subcomplex
Particles	214,408	643,224 (symmetry expanded)
Symmetry	C3	C1
Map sharpening B-factor	-81.8	-94.6
Unmasked resolution at 0.5 FSC (Å)	3.69	3.56
Masked resolution at 0.5 FSC (Å)	3.06	3.25
Unmasked resolution at 0.143 FSC (Å)	3.20	3.28
Masked resolution at 0.143 FSC (Å)	2.69	2.78

Model refinement and validation statistics

Refinement package	Phenix
Refinement tool	Real-space refinement

Refinement strategies

min global, local_grid_search, adp, ss
restraints, rotamer restraints,
Ramachandran restraints

Composition

Amino acids	428
RMSD bonds (Å)	0.004
RMSD angles (°)	0.87
Average B-factors	
Amino acids	99.08
Ramachandran	
Favored (%)	96.23
Allowed (%)	3.79
Outliers (%)	0
Rotamer outliers (%)	0
Clash score	1.37
C-beta outliers (%)	0
CaBLAM outliers (%)	2.16
CC (mask)	0.83
MolProbity score	1.12
EMRinger score	4.38

877

878

879

880

881

882

883

884

885 **DECLARATIONS OF INTEREST**

886 A.R.S. and I.S.G. are co-founders of AbSeek Bio. K.J.K, A.R.S., N.V.J, I.S.G, J.S.M., R.H.C.,
887 and J.E.C. are listed as inventors on patents filed describing the antibodies discovered here.

888 R.H.C. is an inventor on patents related to other SARS-CoV-2 antibodies.

889 J.E.C. has served as a consultant for Luna Biologics, is a member of the Scientific Advisory
890 Boards of CompuVax and Meissa Vaccines and is Founder of IDBiologics. The Crowe
891 laboratory at Vanderbilt University Medical Center has received sponsored research
892 agreements from Takeda Vaccines, IDBiologics and AstraZeneca. J.K.W, E.D. and B.J.D. are
893 employees of Integral Molecular. B.J.D. is a shareholder of Integral Molecular.

894

895

896 **FUNDING**

897 This work was supported by NIAID/NIH grants R01AI131722-S1 (I.S.G.), R01 AI157155
898 (J.E.C.), R01 AI127521 (J.S.M.), T32 AI095202 (S.J.Z.); HHSN contracts 75N93019C00074
899 (J.E.C.), DARPA HR0011-18-2-0001 (J.E.C.), HHSN 75N93019C00073 (B.J.D.); Hays
900 Foundation COVID-19 Research Fund (I.S.G.); Fast Grants (I.S.G.); the Dolly Parton COVID-19
901 Research Fund at Vanderbilt (J.E.C.); Welch Foundation grant number F-0003-19620604
902 (J.S.M.) and Fast Grants, Mercatus Center, George Mason University (J.E.C.). J.E.C. is a
903 recipient of the 2019 Future Insight Prize from Merck KGaA. The Sauer Structural Biology
904 Laboratory is supported by The University of Texas College of Natural Sciences and by award
905 RR160023 from the Cancer Prevention and Research Institute of Texas (CPRIT). The content is
906 solely the responsibility of the authors and does not represent the official views of the U.S.
907 government or other sponsors.

909 REFERENCES

- 910 Adams, P.D., Grosse-Kunstleve, R.W., Hung, L.W., Ioerger, T.R., McCoy, A.J., Moriarty, N.W.,
911 Read, R.J., Sacchettini, J.C., Sauter, N.K., and Terwilliger, T.C. (2002). PHENIX: building new
912 software for automated crystallographic structure determination. *Acta Crystallogr D Biol*
913 *Crystallogr* 58, 1948-1954.
- 914 Alamyar, E., Duroux, P., Lefranc, M.P., and Giudicelli, V. (2012). IMGT((R)) tools for the
915 nucleotide analysis of immunoglobulin (IG) and T cell receptor (TR) V-(D)-J repertoires,
916 polymorphisms, and IG mutations: IMGT/V-QUEST and IMGT/HighV-QUEST for NGS. *Methods*
917 *Mol Biol* 882, 569-604.
- 918 Alpert, T., Brito, A.F., Lasek-Nesselquist, E., Rothman, J., Valesano, A.L., MacKay, M.J.,
919 Petrone, M.E., Breban, M.I., Watkins, A.E., Vogels, C.B.F., *et al.* (2021). Early introductions and
920 transmission of SARS-CoV-2 variant B.1.1.7 in the United States. *Cell*.
- 921 Barnes, C.O., Jette, C.A., Abernathy, M.E., Dam, K.A., Esswein, S.R., Gristick, H.B., Malyutin,
922 A.G., Sharaf, N.G., Huey-Tubman, K.E., Lee, Y.E., *et al.* (2020). SARS-CoV-2 neutralizing
923 antibody structures inform therapeutic strategies. *Nature* 588, 682-687.
- 924 Brouwer, P.J.M., Caniels, T.G., van der Straten, K., Snitselaar, J.L., Aldon, Y., Bangaru, S.,
925 Torres, J.L., Okba, N.M.A., Claireaux, M., Kerster, G., *et al.* (2020). Potent neutralizing
926 antibodies from COVID-19 patients define multiple targets of vulnerability. *Science* 369, 643-
927 650.
- 928 Case, J.B., Rothlauf, P.W., Chen, R.E., Liu, Z., Zhao, H., Kim, A.S., Bloyet, L.M., Zeng, Q.,
929 Tahan, S., Droit, L., *et al.* (2020). Neutralizing Antibody and Soluble ACE2 Inhibition of a
930 Replication-Competent VSV-SARS-CoV-2 and a Clinical Isolate of SARS-CoV-2. *Cell Host*
931 *Microbe* 28, 475-485 e475.
- 932 Chen, R.E., Zhang, X., Case, J.B., Winkler, E.S., Liu, Y., VanBlargan, L.A., Liu, J., Errico, J.M.,
933 Xie, X., Suryadevara, N., *et al.* (2021). Resistance of SARS-CoV-2 variants to neutralization by
934 monoclonal and serum-derived polyclonal antibodies. *Nat Med* 27, 717-726.
- 935 Chi, X., Yan, R., Zhang, J., Zhang, G., Zhang, Y., Hao, M., Zhang, Z., Fan, P., Dong, Y., Yang,
936 Y., *et al.* (2020). A neutralizing human antibody binds to the N-terminal domain of the Spike
937 protein of SARS-CoV-2. *Science* 369, 650-655.
- 938 Cianfrocco, M., Wong, M., Youn, C. COSMIC2 (2017a). COSMIC2 - A Science gateway for
939 cryo-electron microscopy.
- 940 Cianfrocco, M.A., Wong-Barnum, M., Youn, C., Wagner, R. & Leschzinger, A (2017b).
941 COSMIC2: A Science Gateway for Cryo-Electron Microscopy Structure Determination in
942 Proceedings of the Practice and Experience in Advanced Research Computing 2017 on
943 Sustainability, Success, and Impact 1-5. Association for Computing Machinery.
- 944 Croll, T.I. (2018). ISOLDE: a physically realistic environment for model building into low-
945 resolution electron-density maps. *Acta Crystallogr D Struct Biol* 74, 519-530.
- 946 Davidson, E.D., B. J. (2014). A high-throughput shotgun mutagenesis approach to mapping B-
947 cell antibody epitopes. *Immunology* 143, 13-20.
- 948 Dejnirattisai, W., Zhou, D., Ginn, H.M., Duyvesteyn, H.M.E., Supasa, P., Case, J.B., Zhao, Y.,
949 Walter, T.S., Mentzer, A.J., Liu, C., *et al.* (2021). The antigenic anatomy of SARS-CoV-2
950 receptor binding domain. *Cell* 184, 2183-2200 e2122.
- 951 Dong, J., Zost, S.J., Greaney, A.J., Starr, T.N., Dingens, A.S., Chen, E.C., Chen, R.E., Case,
952 J.B., Sutton, R.E., Gilchuk, P., *et al.* (2021). Genetic and structural basis for recognition of
953 SARS-CoV-2 spike protein by a two-antibody cocktail. *bioRxiv*.
- 954 Dunbar, J., Krawczyk, K., Leem, J., Marks, C., Nowak, J., Regep, C., Georges, G., Kelm, S.,
955 Popovic, B., and Deane, C.M. (2016). SAbPred: a structure-based antibody prediction server.
956 *Nucleic Acids Res* 44, W474-478.

957 Elbe, S.B.-M., G. (2017). Data, disease and diplomacy: GISAID's innovative contribution to
958 global health. *Glob Chall* 1, 33-46.

959 Emsley, P., and Cowtan, K. (2004). Coot: model-building tools for molecular graphics. *Acta*
960 *Crystallogr D Biol Crystallogr* 60, 2126-2132.

961 Greaney et al, T.N.S., Christopher O. Barnes, Yiska Weisblum, Fabian Schmidt, Marina
962 Caskey, Christian Gaebler, Alice Cho, Marianna Agudelo, Shlomo Finklin, Zijun Wang, Daniel
963 Poston, Frauke Muecksch, Theodora Hatziioannou, Paul D. Bieniasz, Davide F. Robbiani,
964 Michel C. Nussenzweig, Pamela J. Bjorkman, Jesse D. Bloom (2021). Mutational escape from
965 the polyclonal antibody response to SARS-CoV-2 infection is largely shaped by a single class of
966 antibodies. *BioRxiv*.

967 Gupta, N.T., Vander Heiden, J.A., Uduman, M., Gadala-Maria, D., Yaari, G., and Kleinstein,
968 S.H. (2015). Change-O: a toolkit for analyzing large-scale B cell immunoglobulin repertoire
969 sequencing data. *Bioinformatics* 31, 3356-3358.

970 Hansen, J., Baum, A., Pascal, K.E., Russo, V., Giordano, S., Wloga, E., Fulton, B.O., Yan, Y.,
971 Koon, K., Patel, K., *et al.* (2020). Studies in humanized mice and convalescent humans yield a
972 SARS-CoV-2 antibody cocktail. *Science* 369, 1010-1014.

973 Henderson, R., Edwards, R.J., Mansouri, K., Janowska, K., Stalls, V., Gobeil, S.M.C., Kopp, M.,
974 Li, D., Parks, R., Hsu, A.L., *et al.* (2020). Controlling the SARS-CoV-2 spike glycoprotein
975 conformation. *Nat Struct Mol Biol* 27, 925-933.

976 Hoffmann, M., Arora, P., Gross, R., Seidel, A., Hornich, B.F., Hahn, A.S., Kruger, N., Graichen,
977 L., Hofmann-Winkler, H., Kempf, A., *et al.* (2021). SARS-CoV-2 variants B.1.351 and P.1
978 escape from neutralizing antibodies. *Cell* 184, 2384-2393 e2312.

979 Hsieh, C.L., Goldsmith, J.A., Schaub, J.M., DiVenere, A.M., Kuo, H.C., Javanmardi, K., Le,
980 K.C., Wrapp, D., Lee, A.G., Liu, Y., *et al.* (2020). Structure-based design of prefusion-stabilized
981 SARS-CoV-2 spikes. *Science* 369, 1501-1505.

982 Jones, B.E., Brown-Augsburger, P.L., Corbett, K.S., Westendorf, K., Davies, J., Cujec, T.P.,
983 Wiethoff, C.M., Blackbourne, J.L., Heinz, B.A., Foster, D., *et al.* (2021). The neutralizing
984 antibody, LY-CoV555, protects against SARS-CoV-2 infection in non-human primates. *Sci*
985 *Transl Med*.

986 Kuzmina, A., Khalaila, Y., Voloshin, O., Keren-Naus, A., Boehm-Cohen, L., Raviv, Y., Shemer-
987 Avni, Y., Rosenberg, E., and Taube, R. (2021). SARS-CoV-2 spike variants exhibit differential
988 infectivity and neutralization resistance to convalescent or post-vaccination sera. *Cell Host*
989 *Microbe* 29, 522-528 e522.

990 Li, F. (2016). Structure, Function, and Evolution of Coronavirus Spike Proteins. *Annu Rev Virol*
991 3, 237-261.

992 Liu, L., Wang, P., Nair, M.S., Yu, J., Rapp, M., Wang, Q., Luo, Y., Chan, J.F., Sahi, V.,
993 Figueroa, A., *et al.* (2020). Potent neutralizing antibodies against multiple epitopes on SARS-
994 CoV-2 spike. *Nature* 584, 450-456.

995 Nielsen, S.C.A., Yang, F., Jackson, K.J.L., Hoh, R.A., Roltgen, K., Jean, G.H., Stevens, B.A.,
996 Lee, J.Y., Rustagi, A., Rogers, A.J., *et al.* (2020). Human B Cell Clonal Expansion and
997 Convergent Antibody Responses to SARS-CoV-2. *Cell Host Microbe* 28, 516-525 e515.

998 Pettersen, E.F., Goddard, T.D., Huang, C.C., Meng, E.C., Couch, G.S., Croll, T.I., Morris, J.H.,
999 and Ferrin, T.E. (2021). UCSF ChimeraX: Structure visualization for researchers, educators,
1000 and developers. *Protein Sci* 30, 70-82.

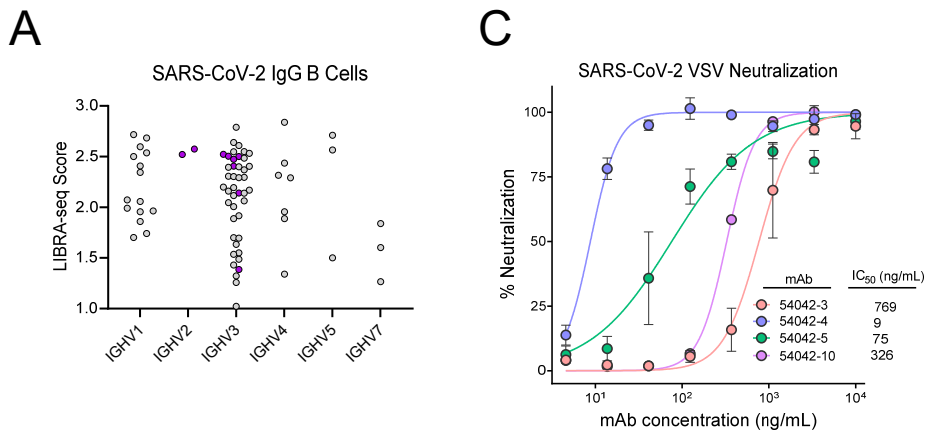
1001 Piccoli, L., Park, Y.J., Tortorici, M.A., Czudnochowski, N., Walls, A.C., Beltramello, M., Silacci-
1002 Fregni, C., Pinto, D., Rosen, L.E., Bowen, J.E., *et al.* (2020). Mapping Neutralizing and
1003 Immunodominant Sites on the SARS-CoV-2 Spike Receptor-Binding Domain by Structure-
1004 Guided High-Resolution Serology. *Cell* 183, 1024-1042 e1021.

1005 Pinto, D., Park, Y.J., Beltramello, M., Walls, A.C., Tortorici, M.A., Bianchi, S., Jaconi, S., Culap,
1006 K., Zatta, F., De Marco, A., *et al.* (2020). Cross-neutralization of SARS-CoV-2 by a human
1007 monoclonal SARS-CoV antibody. *Nature* 583, 290-295.

1008 Punjani, A., Rubinstein, J.L., Fleet, D.J., and Brubaker, M.A. (2017). cryoSPARC: algorithms for
1009 rapid unsupervised cryo-EM structure determination. *Nat Methods* 14, 290-296.
1010 Punjani, A., Zhang, H., and Fleet, D.J. (2020). Non-uniform refinement: adaptive regularization
1011 improves single-particle cryo-EM reconstruction. *Nat Methods* 17, 1214-1221.
1012 Raybould, M.I.J., Kovaltsuk, A., Marks, C., and Deane, C.M. (2021). CoV-AbDab: the
1013 coronavirus antibody database. *Bioinformatics* 37, 734-735.
1014 Rubinstein, J.L., and Brubaker, M.A. (2015). Alignment of cryo-EM movies of individual particles
1015 by optimization of image translations. *J Struct Biol* 192, 188-195.
1016 Sabino, E.C., Buss, L.F., Carvalho, M.P.S., Prete, C.A., Jr., Crispim, M.A.E., Fraiji, N.A.,
1017 Pereira, R.H.M., Parag, K.V., da Silva Peixoto, P., Kraemer, M.U.G., *et al.* (2021). Resurgence
1018 of COVID-19 in Manaus, Brazil, despite high seroprevalence. *Lancet* 397, 452-455.
1019 Sanchez-Garcia, J.G.-B., A Cuervo, JM Carazo, COS Sorzano, J Vargas (2021).
1020 DeepEMhancer: a deep learning solution for cryo-EM volume post-processing. *BioRxiv*.
1021 Setliff, I., Shiakolas, A.R., Pilewski, K.A., Murji, A.A., Mapengo, R.E., Janowska, K., Richardson,
1022 S., Oosthuysen, C., Raju, N., Ronsard, L., *et al.* (2019). High-Throughput Mapping of B Cell
1023 Receptor Sequences to Antigen Specificity. *Cell* 179, 1636-1646 e1615.
1024 Shang, J., Ye, G., Shi, K., Wan, Y., Luo, C., Aihara, H., Geng, Q., Auerbach, A., and Li, F.
1025 (2020). Structural basis of receptor recognition by SARS-CoV-2. *Nature* 581, 221-224.
1026 Shiakolas, A.R., Kramer, K.J., Wrapp, D., Richardson, S.I., Schafer, A., Wall, S., Wang, N.,
1027 Janowska, K., Pilewski, K.A., Venkat, R., *et al.* (2020). Cross-reactive coronavirus antibodies
1028 with diverse epitope specificities and extra-neutralization functions. *bioRxiv*.
1029 Starr, T.N., Greaney, A.J., Hilton, S.K., Ellis, D., Crawford, K.H.D., Dingens, A.S., Navarro, M.J.,
1030 Bowen, J.E., Tortorici, M.A., Walls, A.C., *et al.* (2020). Deep Mutational Scanning of SARS-CoV-
1031 2 Receptor Binding Domain Reveals Constraints on Folding and ACE2 Binding. *Cell* 182, 1295-
1032 1310 e1220.
1033 Suryadevara, N., Shrihari, S., Gilchuk, P., VanBlargan, L.A., Binshtein, E., Zost, S.J., Nargi,
1034 R.S., Sutton, R.E., Winkler, E.S., Chen, E.C., *et al.* (2021). Neutralizing and protective human
1035 monoclonal antibodies recognizing the N-terminal domain of the SARS-CoV-2 spike protein.
1036 *Cell* 184, 2316-2331 e2315.
1037 Tegally, H., Wilkinson, E., Giovanetti, M., Iranzadeh, A., Fonseca, V., Giandhari, J., Doolabh,
1038 D., Pillay, S., San, E.J., Msomi, N., *et al.* (2021). Detection of a SARS-CoV-2 variant of concern
1039 in South Africa. *Nature* 592, 438-443.
1040 Thomson, E.C., Rosen, L.E., Shepherd, J.G., Spreafico, R., da Silva Filipe, A., Wojcechowskyj,
1041 J.A., Davis, C., Piccoli, L., Pascall, D.J., Dillen, J., *et al.* (2021). Circulating SARS-CoV-2 spike
1042 N439K variants maintain fitness while evading antibody-mediated immunity. *Cell* 184, 1171-
1043 1187 e1120.
1044 Tortorici, M.A., and Veesler, D. (2019). Structural insights into coronavirus entry. *Adv Virus Res*
1045 105, 93-116.
1046 Wadman, J.C. (2021). Novavax vaccine delivers 89% efficacy against COVID-19 in U.K.—but is
1047 less potent in South Africa. *Science*.
1048 Wang, P., Nair, M.S., Liu, L., Iketani, S., Luo, Y., Guo, Y., Wang, M., Yu, J., Zhang, B., Kwong,
1049 P.D., *et al.* (2021). Antibody resistance of SARS-CoV-2 variants B.1.351 and B.1.1.7. *Nature*
1050 593, 130-135.
1051 Wec, A.Z., Wrapp, D., Herbert, A.S., Maurer, D., Haslwanter, D., Sakharkar, M., Jangra, R.K.,
1052 Dieterle, M.E., Lilov, A., Huang, D., *et al.* (2020). Broad sarbecovirus neutralizing antibodies
1053 define a key site of vulnerability on the SARS-CoV-2 spike protein. *bioRxiv*.
1054 Weinreich, D.M., Sivapalasingam, S., Norton, T., Ali, S., Gao, H., Bhore, R., Musser, B.J., Soo,
1055 Y., Rofail, D., Im, J., *et al.* (2021). REGN-COV2, a Neutralizing Antibody Cocktail, in Outpatients
1056 with Covid-19. *N Engl J Med* 384, 238-251.

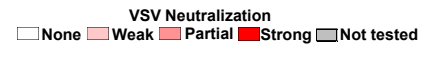
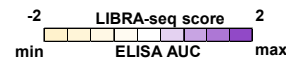
1057 Wrapp, D., Wang, N., Corbett, K.S., Goldsmith, J.A., Hsieh, C.L., Abiona, O., Graham, B.S., and
1058 McLellan, J.S. (2020). Cryo-EM structure of the 2019-nCoV spike in the prefusion conformation.
1059 *Science* 367, 1260-1263.
1060 Xie, X., Liu, Y., Liu, J., Zhang, X., Zou, J., Fontes-Garfias, C.R., Xia, H., Swanson, K.A., Cutler,
1061 M., Cooper, D., *et al.* (2021). Neutralization of SARS-CoV-2 spike 69/70 deletion, E484K and
1062 N501Y variants by BNT162b2 vaccine-elicited sera. *Nat Med* 27, 620-621.
1063 Yuan, M., Liu, H., Wu, N.C., Lee, C.D., Zhu, X., Zhao, F., Huang, D., Yu, W., Hua, Y., Tien, H.,
1064 *et al.* (2020a). Structural basis of a shared antibody response to SARS-CoV-2. *Science* 369,
1065 1119-1123.
1066 Yuan, M., Wu, N.C., Zhu, X., Lee, C.D., So, R.T.Y., Lv, H., Mok, C.K.P., and Wilson, I.A.
1067 (2020b). A highly conserved cryptic epitope in the receptor binding domains of SARS-CoV-2
1068 and SARS-CoV. *Science* 368, 630-633.
1069 Zost, S.J., Gilchuk, P., Chen, R.E., Case, J.B., Reidy, J.X., Trivette, A., Nargi, R.S., Sutton,
1070 R.E., Suryadevara, N., Chen, E.C., *et al.* (2020). Rapid isolation and profiling of a diverse panel
1071 of human monoclonal antibodies targeting the SARS-CoV-2 spike protein. *Nat Med* 26, 1422-
1072 1427.

1073




B

Name	VH gene	VH % identity	CDRH3 length	VDJ junction	VL gene	VL % identity	CDRL3 length	VJ junction	Native isotype	LIBRA-seq scores			ELISA SARS2 S AUC	HT VSV Neut
										SARS2 S	HA NC99	ZM197 Env		
54042-2	IGHV3-30	91.32	21	AKDDGYCLGRGCYYAPGPH	IGLV3-10	94.62	14	YSTDSSGNQNYV	IGHG2					
54042-3	IGHV3-53	96.49	25	ARVHFRYYDDSGYYEANPWFFDL	IGLV1-40	95.83	13	QSYDSSLASAWV	IGHG1					
54042-4	IGHV2-5	97.25	17	AHGLFSSSDWGGGLDV	IGKV1-39	96.42	11	QQSHSTPFI	IGHG1					
54042-5	IGHV2-70	96.91	16	ARVRLGGFDYYMDV	IGLV1-51	97.19	13	GTWDNNLNTGV	IGHG1					
54042-7	IGHV3-9	95.49	18	VRGFREFLKTSGPN DY	IGLV1-51	98.25	13	GTWDGSLSVYV	IGHG1					
54042-10	IGHV3-53	94.74	14	ARDLNVRGGGLDV	IGKV1-9	98.57	12	QQLNSDPALT	IGHG1					
54042-11	IGHV3-53	95.44	13	ARDLVYYGMDV	IGKV1-9	97.85	12	QQVDSYSPFT	IGHG1					
54042-14	IGHV3-33	95.49	23	AKDTWDVPAANPPYSFYMDV	IGKV3-11	98.57	10	QQRSTLIT	IGHG1					
54042-15	IGHV3-9	95.14	16	AKDRLKTGPGYFDL	IGKV3-11	98.57	10	QQRSDWLT	IGHG1					

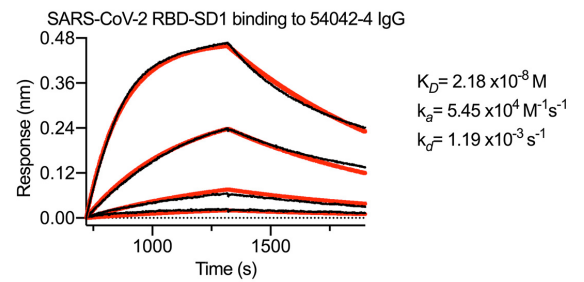


A

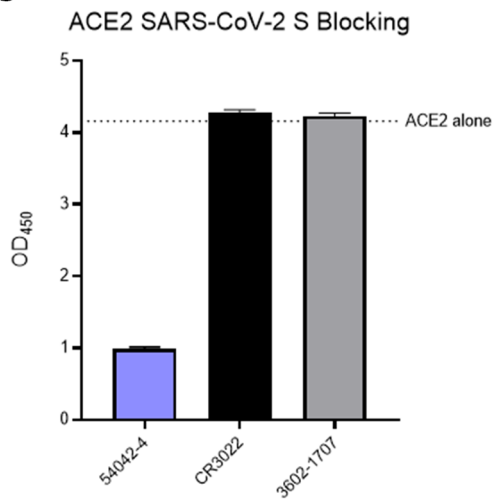
SARS-CoV-2 S Domain	54042-4	CR3022	46472-6	46472-4	3602-1707
RBD					
NTD					
S1					
S2					

ELISA AUC
min  max

B



C



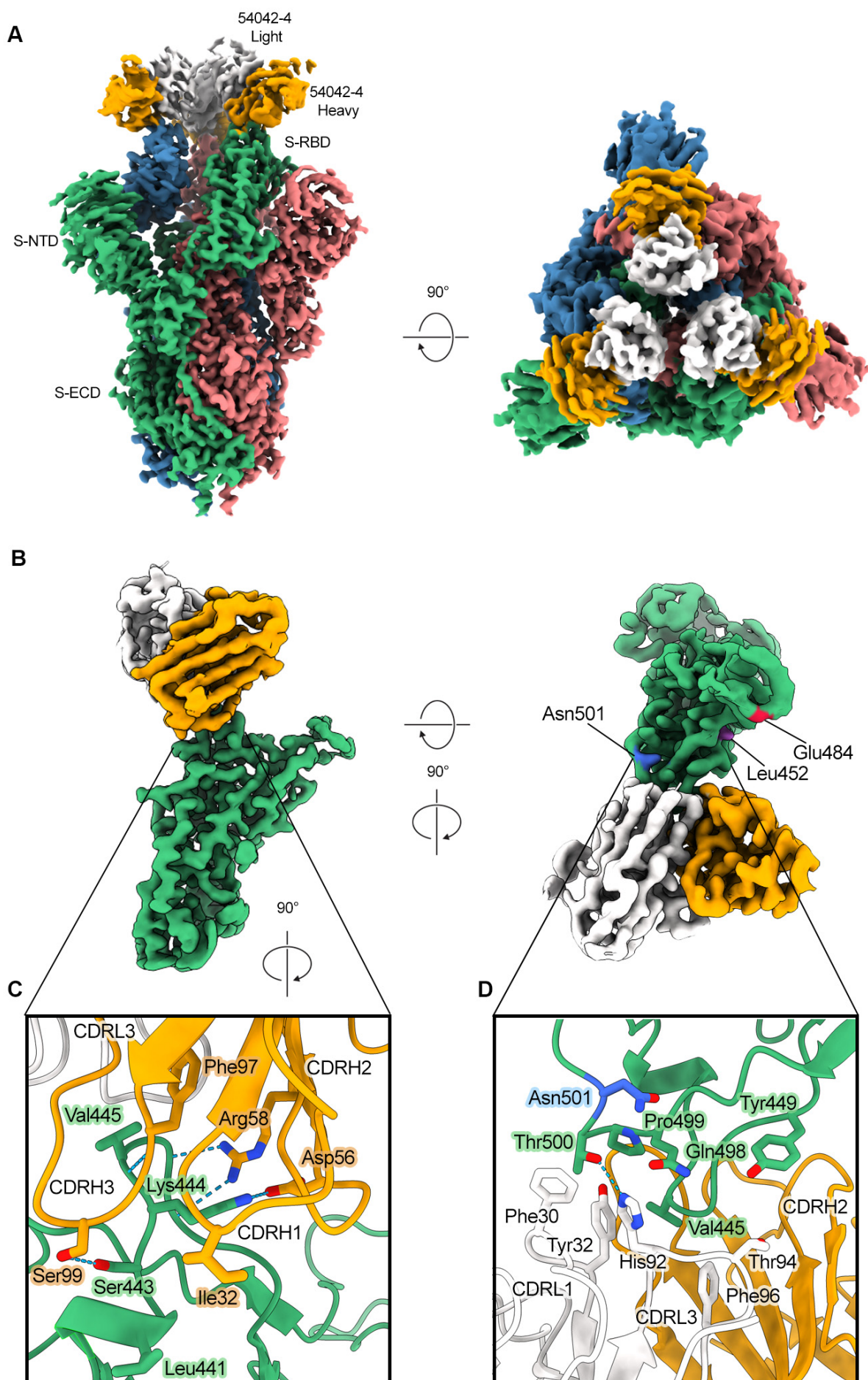
D

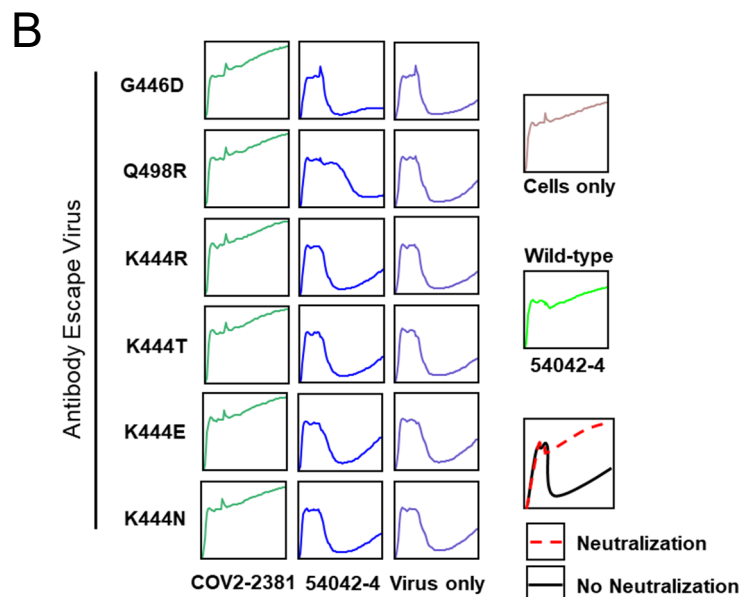
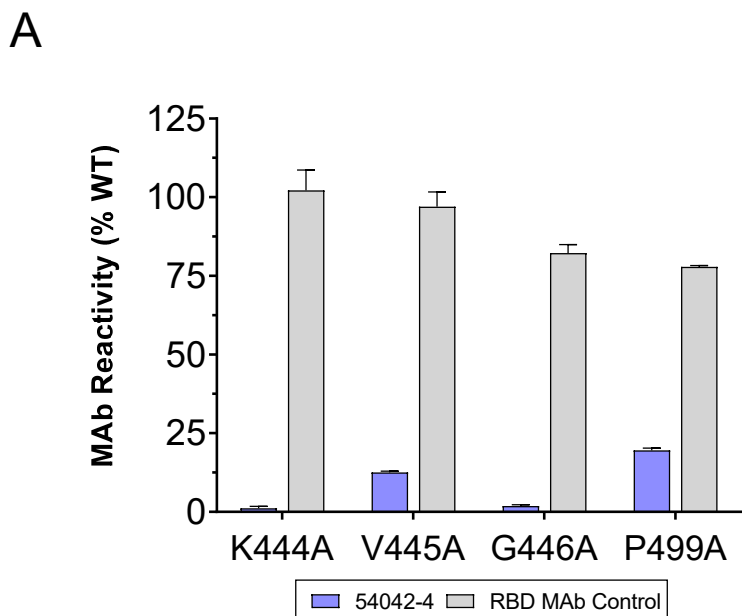
Competitor antibody

mAb	COV2-2196	COV2-2130	54042-4	CR3022
COV2-2196	5	108	106	62
COV2-2130	90	3	15	75
54042-4	78	0	7	76
CR3022	105	95	106	8

Reference antibody

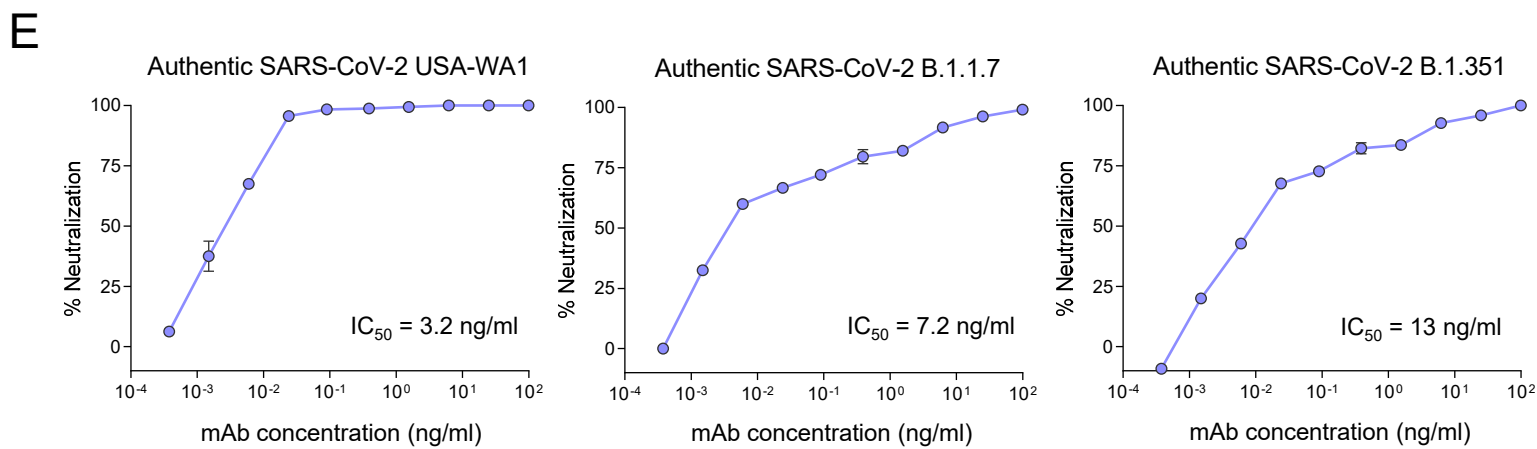
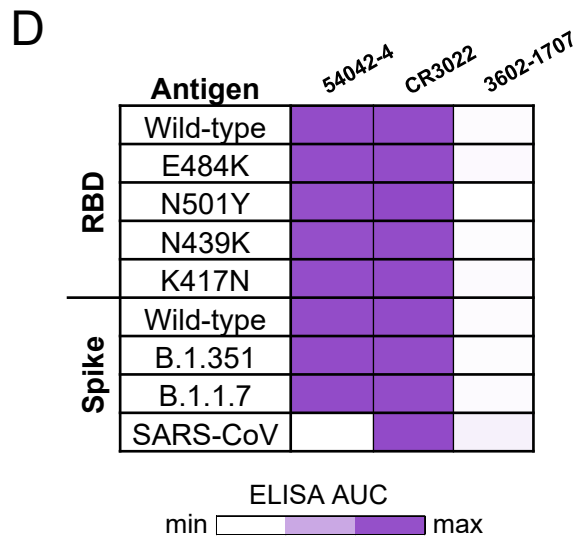
No competition Competition

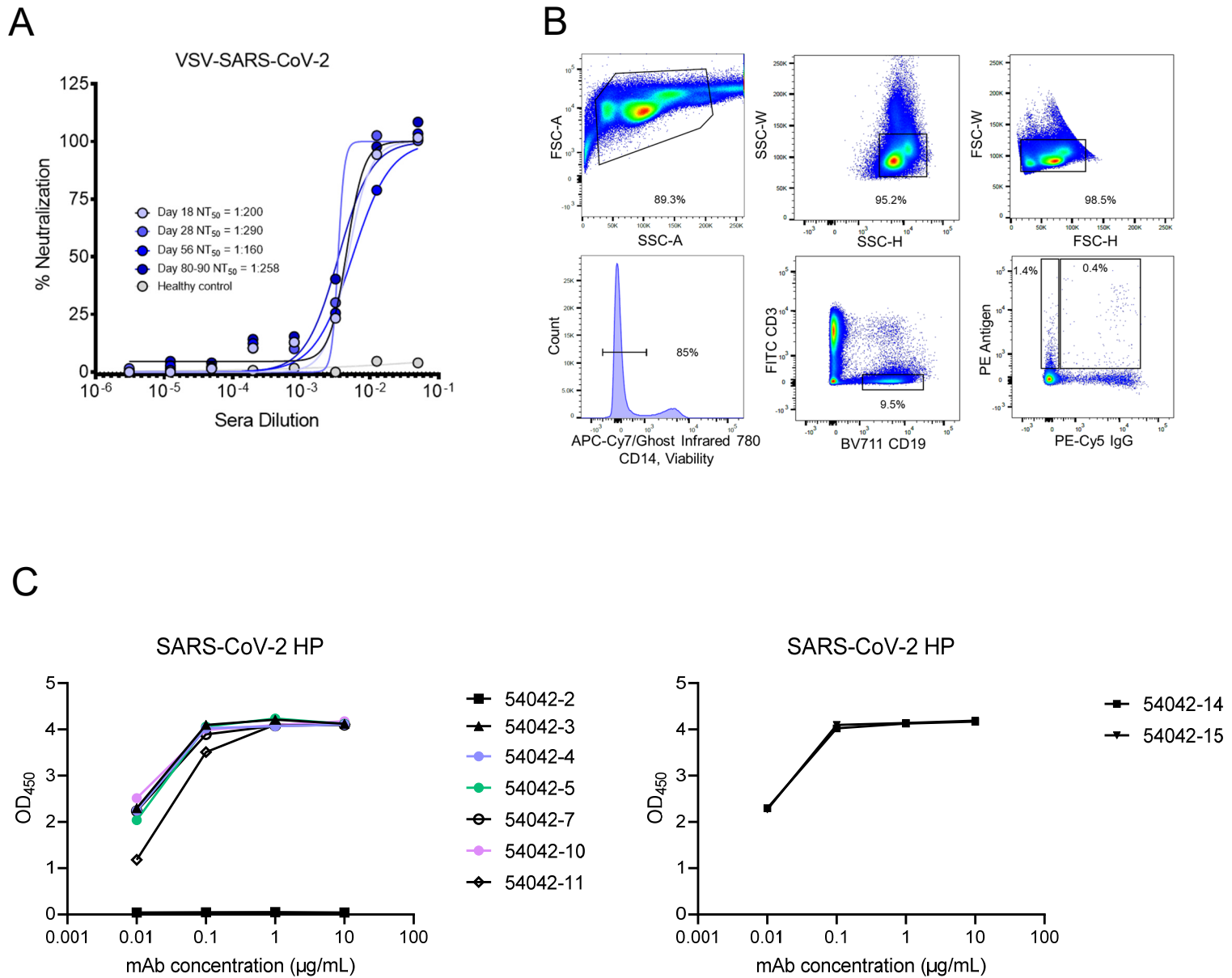


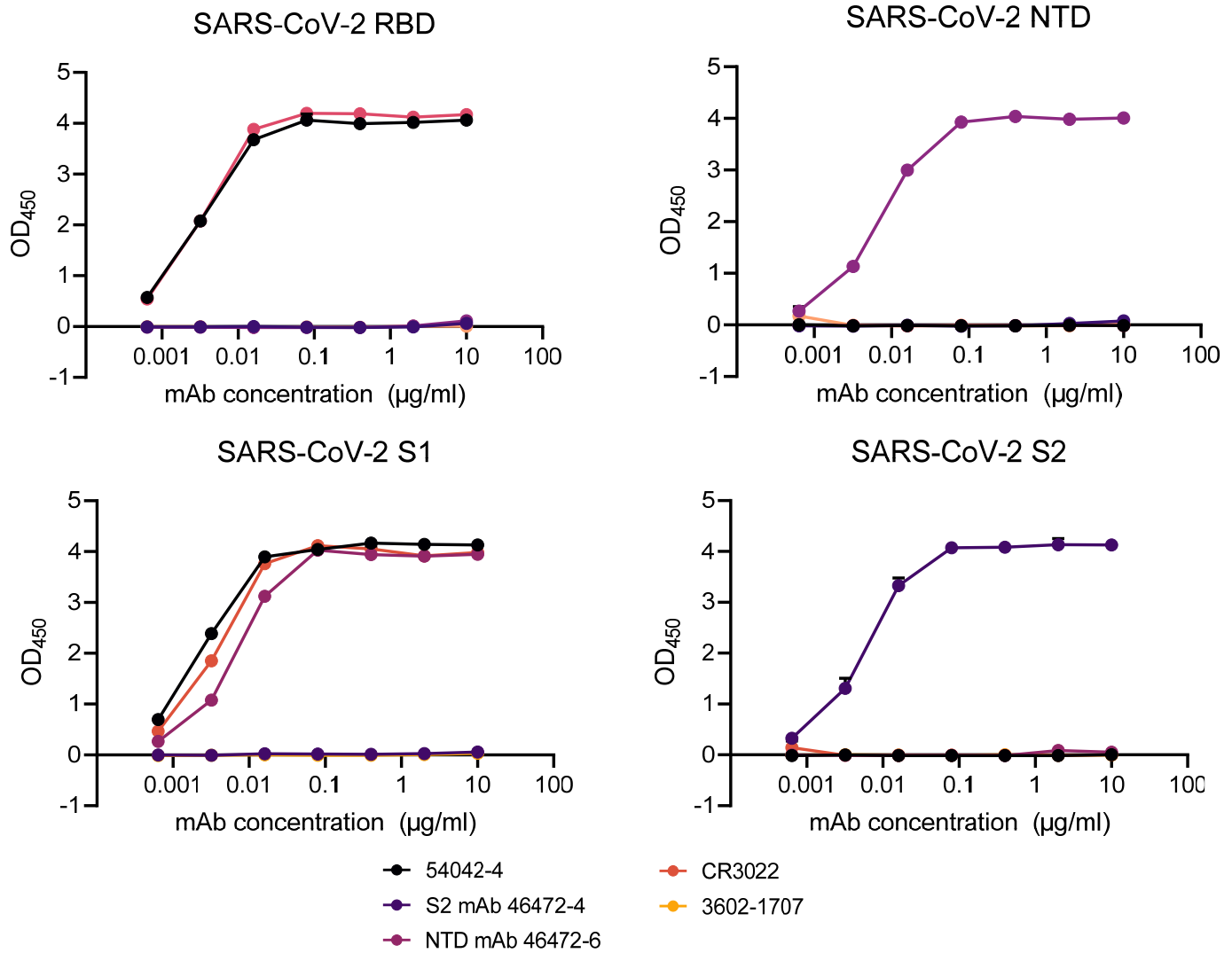


C

54042-4 Epitope Residue	% Conservation
R346	99.183
N439	97.881
N440	99.689
L441	99.846
S443	99.859
K444	99.829
V445	99.676
G446	99.617
G447	99.632
N448	99.564
Y449	99.614
N450	99.570
Q498	99.699
P499	99.693
T500	99.694







A

54042-4 epitope on SARS-CoV-2 S

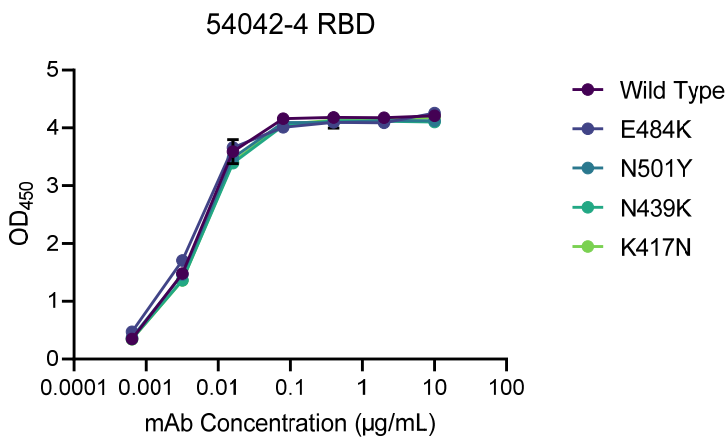
S residue #	AA	Buried surface area
346	R	23
439	N	6
440	N	26
441	L	28
443	S	21
444	K	108
445	V	145
446	G	61
447	G	10
448	N	1
449	Y	33
450	N	48
498	Q	34
499	P	35
500	T	82

B

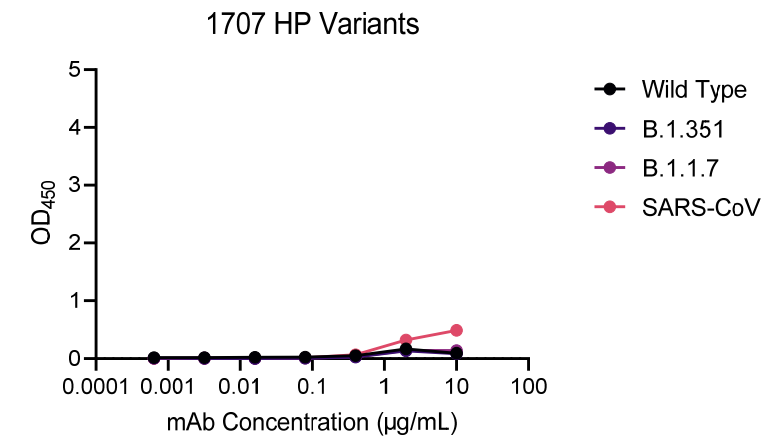
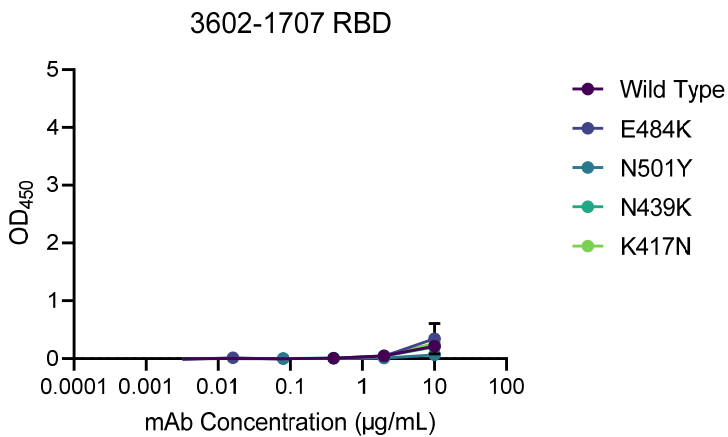
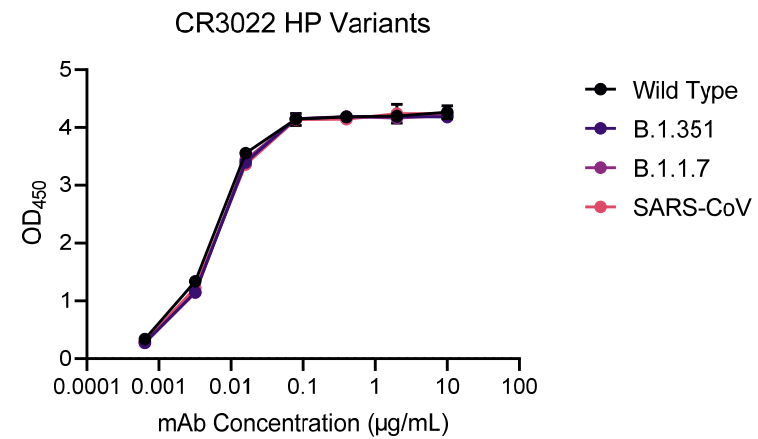
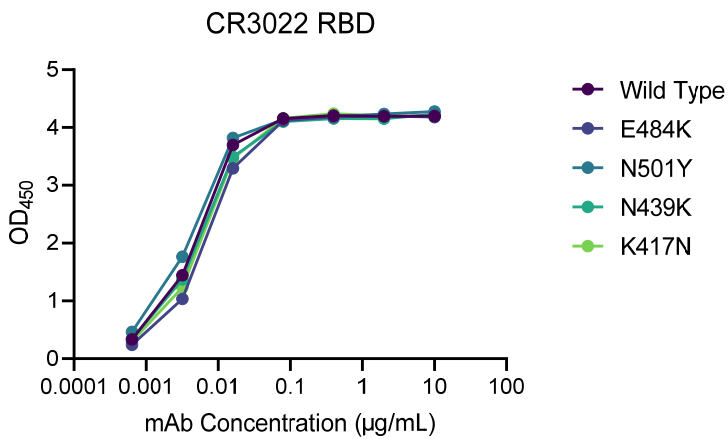
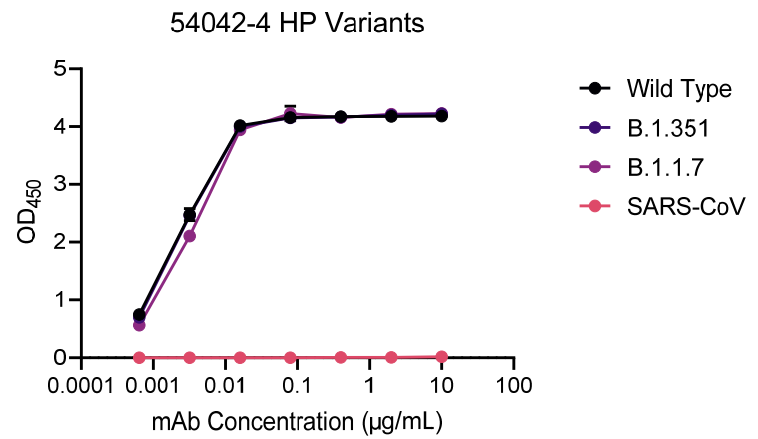
54042-4 paratope on SARS-CoV-2 S

	Ab residue #	AA	Buried surface area	
	32	I	12	
	52	Y	34	
	53	W	42	
	54	D	47	
Heavy chain	56	D	42	
	58	R	61	
	97	F	28	
	98	S	11	
	99	S	99	
	100A	D	2	
	100B	W	2	
	100C	G	2	
		30	F	35
		32	Y	55
Light chain	91	S	10	
	92	H	73	
	93	S	2	
	94	T	20	
	96	F	6	

A



B



C

Mutations in S Variant Constructs

B.1.1.7	B.1.351
Δ69-70	L18F
Δ144	D80A
N501Y	ΔL242-244L
A570D	R246I
P681H	K417N
	E484K
	N501Y

